International journal of spray and combustion dynamics

Original Research Article

International Journal of Spray and Combustion Dynamics
2018, Vol. 10(4) 287–314

DOI: 10.1177/1756827718795518
journals.sagepub.com/home/scd
SAGE

Analytic description of flame intrinsic instability in one-dimensional model of open–open combustors with ideal and non-ideal end boundaries

Nalini Kanta Mukherjee

Abstract

This paper is concerned with the theoretical study of thermo-acoustic instabilities in combustors and focuses upon recently discovered flame intrinsic modes. Here, a complete analytical description of the salient properties of intrinsic modes is provided for a linearized one-dimensional model of open–open combustors with temperature and cross-section jump across the flame taken into account. The standard $n-\tau$ model of heat release is adopted, where n is the interaction index and τ is the time lag. We build upon the recent key finding that for a closed–lopen combustor, on the neutral curve, the intrinsic mode frequencies become completely decoupled from the combustor parameters like cross-section jump, temperature jump and flame location. Here, we show that this remarkable decoupling phenomenon holds not only for closed–open combustors but also for all combustors with the ideal boundary conditions (i.e. closed–open, open–open and closed–closed). Making use of this decoupling phenomenon for the open–open combustors, we derive explicit analytic expressions for the neutral curve of intrinsic mode instability on the $n-\tau$ plane as well as for the linear growth/decay rate near the neutral curve taking into account temperature and cross-section jumps. The instability domain on the $n-\tau$ plane is shown to be qualitatively different from that of the closed–open combustor; in open–open combustors it is not confined for large τ. To find the instability domain and growth rate characteristics for non-ideal open–open boundaries the combustor end boundaries are perturbed and explicit analytical formulae derived and verified by numerics.

Keywords

Flame intrinsic modes, $\eta-\tau$ model, open-open combustors, intrinsic-acoustic mode coupling, thermo-acoustic instabilities

Date received: 3 April 2017; accepted: 9 April 2018

1. Introduction

A major proportion of the energy produced in modern era comes from the combustion of fossil fuels, which is also a dominant contributor to air pollution. Due to stricter pollution norms, combustors are compelled to reduce NO_X by reducing the temperature during combustion. Hence, lean premixed pre-vaporized combustors have been introduced.[1,2] However, it comes at a cost of increased likelihood of thermo-acoustic combustion instability during the combustion process.[3,4] Combustion instabilities can be observed in many systems such as liquid and solid propellant rockets, jet engines, ramjets and industrial power plants. Combustion instability comes to the fore if the gains associated with the non-steady combustion process exceed the losses due to viscous effects, heat transfer, particle relaxation and radiation damping.[5] In general, the gain processes driving combustion instability are diverse and complex, because multiple phenomena should be taken into consideration at once to incorporate three-way coupling between the flame heat release, the acoustics of the combustor and the hydrodynamics.

School of Computing and Mathematics, Keele University, Keele, UK

Corresponding author:
Nalini Kanta Mukherjee, School of Computing and Mathematics, Keele University, Keele ST5 5BG, UK.
Email: nalinikanta65@gmail.com

In engineering practice, it is commonly assumed that the coupling between flame heat release and one of the acoustic modes plays a key role in the advent of thermo-acoustic instabilities in combustors. The present combustion literature offers abundant coverage of the role of acoustic modes in combustion instability. The text books of Lieuwen and Yang,[6] Poinsot and Veynante[7] as well as theoretical work by Dowling et al.[8,9] can be referred in this context for more details.

However, recently, Hoeijmakers et al.[10] and Hoeijmakers[11] discovered a completely new family of modes originating from the localized flame subsystem (flame and air/fuel supply line). These modes are often referred to as the *flame intrinsic thermo-acoustic modes*. Throughout this paper, we call them for brevity just *intrinsic* modes. Hoeijmakers et al.[10] studied these modes analytically using the scattering matrix of the flame itself. The matrix is completely independent of the acoustic boundary conditions. The governing dispersion relation for intrinsic modes was found to be $\varepsilon + 1 + \theta F(\omega) = 0$, where, $F(\omega)$ is the flame transfer function, ε is the ratio of specific acoustic impedance and θ is the jump in temperature across the flame. A simple explicit expression for intrinsic mode frequencies was given as $(\pi \pm 2k\pi)/\tau$, where, τ is the time lag and k is an integer. The critical gain for the intrinsic mode to become unstable in an anechoic environment was found to be $n_c = (\varepsilon + 1)/\theta$, and thus the critical gain depends on the temperature jump. The analytical study was supplemented by numerical analysis of a resonator model. In the literature,[10] it was also shown that the poles of the complete system (flame + acoustics) for acoustic reflections at combustor ends going to zero (i.e. anechoic) are the same as those found for the scattering matrix of the flame, in-line with our expectations. The analytical expression of intrinsic modes for flame in an anechoic environment was also considered in Emmert et al.,[12] where an investigation of the stability features of intrinsic modes was performed based on the balance of the acoustic energy across the flame. In a parallel study, Courtine et al.[13] pointed out that the theoretical predictions of the stability and the frequency of intrinsic modes strongly depend on the flame transfer function. Instability frequencies and spatial structures of the modes, predicted theoretically, were captured by direct numerical simulation (DNS) with good accuracy for the flames with sufficient confinement (small cross-section ratio between injection duct and combustion chamber). It was further confirmed that intrinsic thermo-acoustic modes can be more unstable in confined combustion chambers and thus highlighted the necessity of considering acoustic ends of the combustor in the theoretical models.

In Emmert et al.,[14] it has been shown that acoustic and intrinsic thermo-acoustic modes constitute the complete set of eigen-modes of a combustor. They adopted a numerical approach in identifying intrinsic and acoustic mode frequencies. Most importantly, they reported that increase of acoustic losses at the ends of combustor may destabilize the combustion system because of intrinsic flame instability. This observation is supported by the experiments of Hoeijmakers et al.[15] Hoeijmakers et al.[15] further point out that the effectiveness of passive thermo-acoustic damping devices could be restricted by intrinsic stability properties of flame. Theoretical work of Bomberg et al.[16] also confirms the presence of intrinsic modes. Previous experimental observation of thermo-acoustic instability frequencies made for two different combustors ((a) laminar flame holder-stabilized and (b) turbulent swirl-stabilized burner[17,18]) were interpreted as intrinsic modes by Bomberg et al.[16] via an analytical study of the combustor stability using the flame transfer matrix. Independent DNSs by Courtine et al.[19] and Silva et al.[20] further confirms the intrinsic thermo-acoustic feedback to be an authentic physical phenomenon and not just a spurious by-product of simplistic models. A possible physical mechanism of flame intrinsic modes was pointed out by Hoeijmakers et al.[10] as the creation of localized feedback loop by flame and its nearby environment (i.e. air/fuel supply line).

Thus, the common assumption that in thermo-acoustic instabilities flame heat release always locks onto one of the acoustic modes is not necessarily true. It needs to be critically reconsidered on a case-by-case basis.[16]

The literature review in the previous section identifies and firmly establishes the presence of flame intrinsic modes within combustors. These modes have been neglected for decades in the study of thermo-acoustic instability. Having said that the study of the literature on intrinsic modes is predominantly confined within the computational and experimental domain. The only analytical studies performed in the field so far considers an anechoic chamber[10] and a closed–open combustor model.[21] For an anechoic boundary condition, it has been shown[10] that intrinsic modes can become unstable for certain flame parameters. Having said that, what is the corresponding criterion for intrinsic instability in a practical combustor, is an open question, which requires detailed investigation. Courtine et al.[13] mention that acoustic reflection from the ends of the combustor can further facilitate the instability. But the analytical criterion based on which this phenomenon can be predicted remains to be found yet. In this context, through an analytical and numerical investigation, Hoeijmakers et al.[22] derived bounds for the acoustic losses in the flame surroundings based on which the stability of a thermo-acoustic system can be ensured. The method was illustrated on a couple of premixed

multiple Bunsen type burners. The prediction from the numerical approach was found to be less conservative than the analytical one. In their numerical approach, the upper bound of the acoustic losses were provided as a combination of up and downstream losses, providing flexibility to incorporate additional losses at either end of the combustor, based on design convenience.

In the literature,[21] the analytic study is based on the observation that the dispersion relation can be exactly factorized on the boundary of instability, i.e. the neutral curve.[23] This enables one to find analytically instability domain and the corresponding linear growth/decay rate near its boundary. However, it remained unclear whether this analytical approach can be extended to any other type of combustors and, if yes, what features of the intrinsic mode instabilities in the known combustor models persist and what will change and how. The present work aims to address these questions. We show that the open–open systems also have the remarkable property of factorization of the dispersion relation on the stability boundary, which enables us to answer the key questions concerned with the intrinsic mode instabilities in such systems. To obtain comprehensive picture of stability behaviour of intrinsic modes in a multi-dimensional parameter space via numerics is an extremely challenging and time-consuming assignment, since the effects of the combustor properties (e.g. flame location, boundary conditions at the ends and parameters of the cross-section and temperature jumps) on the intrinsic mode growth rates need to be studied. The current work addresses this need for a one-dimensional (1D) model of open–open combustors with temperature and cross-section jump across the flame.

Here, we consider a standard 1D acoustic model of an open–open combustor with a heat source. The heat release rate is modelled by the linear $n-\tau$ model.[24] Within the framework of this simplified open–open combustor model, we will provide an overall picture of the intrinsic modes and explicit analytical expressions for the key parameters of the intrinsic modes (instability domains in the parameter space, the growth/decay rates, frequencies of unstable modes) for the whole range of the system parameters.

The current work is a follow-up of Mukherjee and Shrira,[21] where a comprehensive analytical study of intrinsic modes has been performed for a 1D quarter wave resonator (ideal closed–open acoustic ends). The work[21] finds the exact intrinsic instability frequency, the exact instability domain in the parameter space and with a good accuracy the corresponding linear growth rate near the neutral curve. An idealized open–open or closed–open assumption for acoustic ends of the combustor is a reasonable first approximation for the purpose of the analytical study. The closed end of the combustor implies choked inlet nozzle for low Mach number,[25] whereas the open end of the combustor implies that the flow goes into the open atmosphere, the reflection coefficient of which is known.[26] The work by Mukherjee and Shrira[21] is based on the assumption of idealized closed–open ends of the combustor, which is a reasonable first approximation for many real combustors. But some real systems could have their idealized prototype as an open–open combustor. The present work focuses on this specific type of combustor. Findings of Mukherjee and Shrira[21] show that for a closed–open combustor, on the neutral curve, the intrinsic mode frequencies become completely decoupled from the combustor parameters like cross-section jump, temperature jump and flame location. This prompts the question on whether this decoupling holds for any other boundary conditions, as well. In this paper, we show that this remarkable decoupling phenomenon occurs only for strictly ideal boundary conditions (i.e. closed–open, open–open and closed–closed). In this regard, we must mention that in an industrial gas turbine combustor there is a compressor assembly in the upstream and turbine assembly in the downstream of the combustor, imposing certain limitations on the validity of the perfectly closed or perfectly open assumption of acoustic ends. A detailed analysis of impedances at acoustic boundaries can be found in Lamarque and Poinsot,[25] Silva et al.[27] and Marble and Candel.[28] Once the intrinsic instability features for combustors with ideal end conditions are known, we obtain the intrinsic instability features for practical systems through linear perturbations of the acoustic ends of an idealized open–open combustor. We find the neutral curve and growth rate for combustor with non-ideal open–open boundaries, and also identify the parameter space where the analytical solution loses its robustness.

The current paper is organized as follows: In Section 2, we develop the mathematical model to derive the acoustic dispersion relation for a combustor with open–open end conditions, taking into account cross-section and temperature jumps across the flame. In Section 3, we examine numerically the behaviour of acoustic and intrinsic modes on the complex frequency plane and identify $n-\tau$ parameter domains where intrinsic instability might be stronger than the acoustic instability. In Section 4, we consider decoupling of intrinsic mode from the combustor parameters for the case of an open–open combustor. Then, we derive an analytical expression for the n-threshold for the intrinsic mode to become unstable, which leads to neutral curves on the $n-\tau$ plane. Further, we arrive at an expression of linear growth/decay rate for an intrinsic mode near the neutral curve. In this section, we also show that the factorization of the dispersion relation on

the neutral curve holds good only for ideal (closed or open) boundary conditions. In Section 5, we linearly perturb the acoustic boundaries of the combustor and obtain the analytical solution of the neutral curve and growth rate for combustor with non-ideal boundaries. In Section 6, we study the effect of various combustor parameters like flame location, cross-section jump and temperature jump on the neutral curves and growth rates. Finally, the concluding comments are given in Section 7.

2. Mathematical model for a combustor with open–open end conditions: Derivation of the dispersion relation

In this paper, we will focus on the analytical study of flame intrinsic modes in a common 1D model of an acoustic open–open combustor. Hoeijmakers et al.[10] provided an analytical description of the intrinsic mode for a flame kept in a tube with anechoic boundary conditions. The results of the analytical study of intrinsic flame modes by Mukherjee et al.[29] were produced for a 1D quarter wave resonator. In the present context, we will restrict our analysis to the simplest case of a combustor with ideal open–open end conditions. The 1D analytical formulation based upon $n-\tau$ model is capable to generate valuable insight into the stability behaviour of intrinsic modes in multi-dimensional parameter space.

Figure 1 provides a schematic sketch of an open–open combustor with a compact heat source at $x = x_q$, with x being the longitudinal coordinate with the origin at the left open end of the combustor. A_1, A_2 and B_1, B_2 are the pressure amplitudes for the forward/backward going waves in the upstream and the downstream region, respectively. The mean temperature is assumed to jump from T_1 to T_2 across the flame. The cross-sectional area jumps across the flame from S_1 to S_2. The current mathematical model is based on the following assumptions:

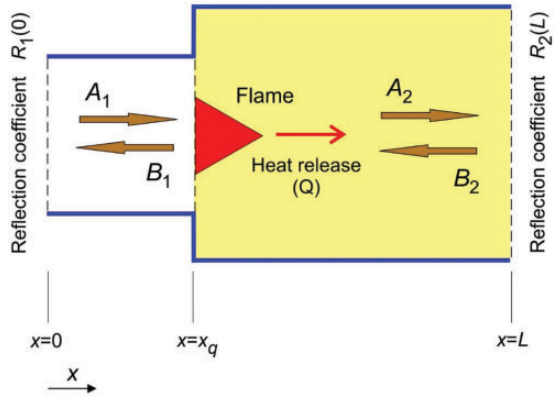

Figure 1. Schematic sketch of a combustor with open–open end conditions. The combustor has a cross-sectional area jump at the flame location $x = x_q$. Thick arrows (brown online) symbolize the forward/backward travelling waves upstream/downstream of the flame. Lightly shaded region (yellow online) marks the domain of higher temperature after the temperature jump across the flame.

(i) We consider a 1D acoustic model and thus the wave is assumed to propagate only in the axial direction (x).
(ii) Both of the end conditions of the combustor are assumed to be ideal open. In practical combustors, reflection coefficients at the boundaries have a dissipative and a reactive part; the reflection coefficients are also frequency dependent. However, we assume the reflection coefficient to be exactly -1 for all frequencies.
(iii) The flame is assumed to lie on a single hypothetical axial plane. Any distribution of the flame (heat release rate) in the axial direction is not considered for the time being.
(iv) The flame heat release rate is modelled by the linear $n-\tau$ law.[24] In general, the flame response is larger at the lower frequencies as compared to the higher frequencies. Consideration of $n-\tau$ flame model, which is based on frequency independent gain of the flame transfer function, hence, does not reflect the true physical reality. This common assumption is adopted here to simplify the analytical model.
(v) Effect of mean flow and the subsequent hydrodynamic instabilities are ignored in this model. We also neglect the effect of turbulence in the model.
(vi) We neglect damping or losses of any kind in the current analytical model.
(vii) In actual combustors, there is a continuous distribution of temperature across the length of the combustor. Non-uniform temperature gives rise to entropy waves in the system.[30] For simplicity, we ignore this distribution of temperature and assume the mean temperature to jump from T_1 to T_2 across the flame. The effect of entropy waves, therefore, is neglected in our model.

The acoustic pressure and particle velocity at the upstream region and at the downstream region of the combustor can be written as[31]

$$\tilde{p}_1(x,t) = \left[A_1 e^{ik_1 x} + B_1 e^{-ik_1 x}\right] e^{-i\omega t},$$
$$\tilde{u}_1(x,t) = \left(\frac{1}{\rho_1 c_1}\right)\left[A_1 e^{ik_1 x} - B_1 e^{-ik_1 x}\right] e^{-i\omega t}, \text{ and}$$

$$\tilde{p}_2(x,t) = \left[A_2 e^{ik_2 x} + B_2 e^{-ik_2 x}\right] e^{-i\omega t},$$
$$\tilde{u}_2(x,t) = \left(\frac{1}{\rho_2 c_2}\right)\left[A_2 e^{ik_2 x} - B_2 e^{-ik_2 x}\right] e^{-i\omega t}$$

The wave numbers k_i ($i = 1, 2$) upstream and downstream of the flame can be presented as $k_1 = \omega/c_1$ and $k_2 = \omega/c_2$, where ω is the complex frequency, c_1, c_2 represent the speed of sound and ρ_1, ρ_2 are the mean densities upstream and downstream of the flame, respectively. For open–open combustor, the boundary conditions at two ends can be represented as follows

$$\text{at } x = 0,\ A_1/B_1 = R_1(0) = -1, \text{ and} \tag{1}$$

$$\text{at } x = L,\ B_2 e^{-ikL}/A_2 e^{ikL} = R_2(L) = -1 \tag{2}$$

The pressure and flow rate balance at $x = x_q$ implies[9,32]

$$\tilde{p}_1(x_q) = \tilde{p}_2(x_q), \text{ and} \tag{3}$$

$$S_1 \tilde{u}_1(x_q) + \left((\gamma - 1)/\rho_1 c_1^2\right)\tilde{Q} = S_2 \tilde{u}_2(x_q) \tag{4}$$

Here, $\tilde{Q}(t)$ is the heat release rate at $x = x_q$ and γ represents the ratio of specific heats of air $\left(c_p/c_v\right)$. It is assumed that the heat source acts like a monopole with a volume outflow $(\gamma - 1)(\tilde{Q}/\rho_1 c_1^2)$.[9] The linear heat release law can be assumed to be of the form (see e.g. Truffin and Poinsot[33]); $\tilde{Q}(t) = \left(\rho_1 S_1 c_1^2/(\gamma - 1)\right) \times n\tilde{u}_1(x_q, t - \tau)$. Here, n and τ are the interaction index and time lag, respectively. The rate of heat release fluctuations, $\tilde{Q}$, is assumed to be proportional to the local velocity upstream of the flame, $\tilde{u}_1$, with a time lag, τ. In the frequency domain, this can be written as,[33] $\tilde{Q}(\omega) = \left(\rho_1 S_1 c_1^2/(\gamma - 1)\right) n e^{i\omega\tau} \tilde{u}_1(x_q, \omega)$.

The set of homogeneous equations for A_1, B_1, A_2 and B_2, equations (1) to (4) are usually presented in the matrix form.[34] However, we arrive at a compact dispersion relation, which provides the basis for all analytical derivations in the subsequent sections (refer Mukherjee and Shrira[21])

$$\begin{aligned}&[(S_2/S_1)(\rho_1/\rho_2)(c_1/c_2) + 1]\sin\left((k_2 - k_1)x_q - k_2 L\right)\\ &\quad + [(S_2/S_1)(\rho_1/\rho_2)(c_1/c_2) - 1]\sin\left(k_2 L - (k_1 + k_2)x_q\right)\\ &\quad + 2ne^{i\omega\tau}\cos k_1 x_q \sin k_2\left(x_q - L\right) = 0\end{aligned} \tag{5}$$

We denote the function on the left-hand side of transcendental equation (5) as $g(\omega)$. Thus, dispersion relation (5) can be re-written compactly as

$$g(\omega) = 0 \tag{6}$$

The dispersion relation can be simplified for special cases, when there is no cross-section and temperature jumps across the flame, that is $S_1 = S_2$ and $T_1 = T_2$, and thus $c_1 = c_2$, $\rho_1 = \rho_2$ and $k_1 = k_2 = k$. For these situations, the dispersion relation (5) reduces to

$$\sin kL - ne^{i\omega\tau}\cos kx_q \sin k\left(x_q - L\right) = 0 \tag{7}$$

The dispersion relation (7) can be further simplified when the flame is located exactly in the centre of the combustor, i.e. at $x_q = L/2$. Specific features for this case will be explored in Section 3.2.

A solution of the dispersion relations (5) and (7) generates the eigen-frequencies ω of the system. Equation (5) describes the most general case (an open–open combustor with a cross-section and temperature jump across the flame), while equation (7) is the reduced versions of equation (5) for special cases. The real part of ω is the frequency, while the imaginary part is the growth/decay rate. The particular form of the dispersion relation (5) and (7) makes them a convenient object for an analytical study. It will be shown in Section 4 that these equations allow factorization (or decoupling from combustor parameters) on the neutral curve and on this basis, we can obtain useful analytical expressions of modal frequency and growth rate near the neutral curve.

3. Intrinsic modes in the general picture of the combustor modes

It has been confirmed by the findings of Hoeijmakers et al.[10] and later by Mukherjee and Shrira[21] that there is always an infinite number of intrinsic mode present in any combustor for any n and τ, whatever might be the end conditions. In the asymptotic limit of small n, these modes are strongly decaying for any 1D combustor with a linear $n - \tau$ model of flame heat release. These modes are independent of the acoustic modes and in the limit of small n these modes are strongly localized and thus do not feel the combustor boundaries and other parameters of the system. An explicit solution for the intrinsic mode frequency for small n for any combustor with linear $n - \tau$ model of flame heat release has been reported by Mukherjee and Shrira[21] as follows

$$\begin{aligned}\omega = &\left(2m^i + 1\right)(\pi/\tau)\\ &- (i/\tau)\ln([(S_2/S_1)(\rho_1/\rho_2)(c_1/c_2) + 1]/n),\end{aligned} \tag{8a}$$

Which can be approximated as,

$$\omega \approx \left(2m^i + 1\right)(\pi/\tau) + (i/\tau)\ln(n) \tag{8b}$$

Here, m^i is the mode number of the flame intrinsic modes. When the cross-section is assumed to be constant, the expression of modal frequency for any combustor in the limit of small n, as given by equation (8a),

is the same as found from the result provided by Hoeijmakers et al.[10] for an infinite tube with a flame inside. Note a difference in the notation: in this paper, n is the same as in Courtine et al.,[13] which relates to n in Hoeijmakers et al.[10] (here labelled as n_H) as $n = \theta n_H$, where $\theta = (T_2/T_1) - 1$. Besides, there is another difference. The expression given by Hoeijmakers et al.[10] is valid for any n (as the effect of combustor boundaries are neglected), whereas in the current paper, equation (8a) is valid only for sufficiently small n. The salient features of equation (8a) are that the intrinsic modes have their own mode numbers, completely independent of the mode numbers of the acoustic modes. The real part of the flame intrinsic mode frequency depends only on the time lag and mode numbers (m^i), whereas the decay rates are independent of the mode numbers and are inversely proportional to τ. For small but finite n the decay rates depend on some of the parameters of the combustor as given explicitly by equation (8a) and do not depend on the end conditions. In the limit of small n, the decay rate depends logarithmically on n. Intrinsic modes, however, have the potential to become unstable once the value of n exceeds a certain threshold, as observed by Mukherjee and Shrira[21] for a closed–open combustor and also, previously, by Hoeijmakers et al.[10] for the case of the flame in an infinite tube.

3.1. Stability features of intrinsic modes: Contour plots on the complex frequency plane

Here, we examine the features of the full dispersion relation (5) numerically. For certainty, we consider as an example a combustor with the parameters of the test rig at IIT Madras:[35,36] the length L is 0.75 m, the cross-section S is 0.0016 m^2, the temperature T is assumed constant throughout the duct and equal to 297 K (the effect of temperature jump will be considered in Sections 4, 5 and 6). For most of our analysis, we assume the flame to be located at $x_q = L/3$. The actual combustor at IIT Madras is closed–open. But in this study, we only use the physical dimensions of the setup. However, we stress that the specific parameters of the combustor are immaterial for our study and they are used for illustration only. Our analytical model is applicable to any open–open combustor (with ideal open end conditions) as long as 1D model idealization retains validity.

To facilitate a simultaneous study of acoustic and intrinsic modes, similar to Mukherjee et al.,[29] we generate contour plots of the absolute value of function $g(\omega)$ prescribed in the full dispersion relation (5) on the complex frequency plane. This enables us to follow the frequencies and the growth/decay rates of the modes at the same time.

In Figures 2 to 4, acoustic modes are marked with squares (blue online), while intrinsic modes are shown by triangles (orange online). The instability domain is marked in lightly shaded (yellow online). The acoustic mode frequencies are $m^a(\pi c/L)$ (for $m^a = 1, 2, \ldots$ and assuming $c_1 = c_2 = c$)[31] and have almost zero growth rates in Figure 2, because the n selected ($n = 0.025$) is very close to zero. The innermost closed loops of the iso-lines of the absolute value of the function $g(\omega)$ in the complex ω plane indicates the solution region for modal frequency ω. The modal frequencies are discrete points corresponding to $|g(\omega)| = 0$ (represented by squares and triangles) in these solution regions. In Figures 2 to 4, we present both dimensional (ω in rad/s) and

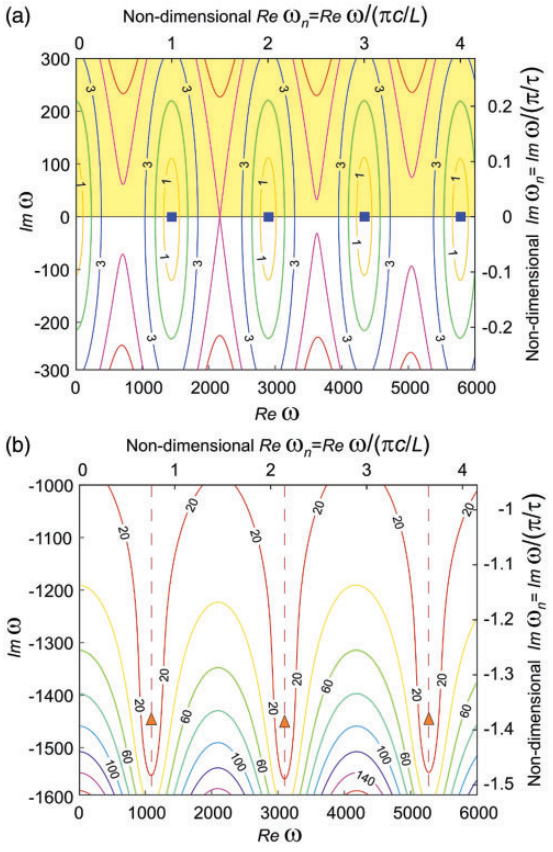

Figure 2. Contour plot of $|g(\omega)|$ for $n = 0.025$, $\tau = 3.0$ ms and $x_q = L/3$ (no temperature and cross-section jump). The parameters used for this plot are from the test rig of IIT Madras[35]: the length L is 0.75 m, the cross-section S is 0.0016 m^2, the temperature T is assumed constant throughout the duct and equal to 297 K. The flame is located at $x_q = L/3$, $c_1 = c_2 = 345$ m/s. Two sections are parts of the same contour plot. The domain of instability is lightly shaded (yellow online). Squares (blue online) and triangles (orange online) represent the acoustic and intrinsic modes, respectively. Thin dashed (red online) vertical lines indicate the intrinsic mode frequency in the limit of small n, given by equation (8b).

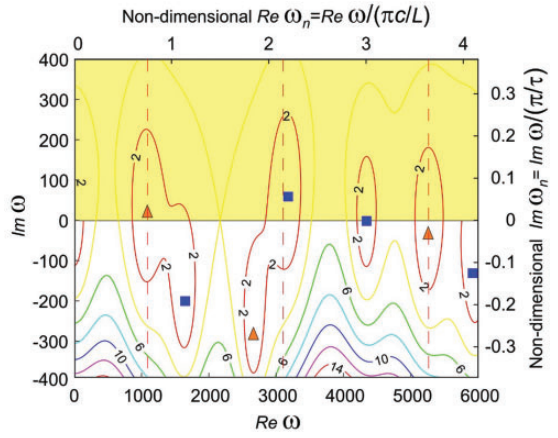

Figure 3. Contour plot of $|g(\omega)|$ for $n = 1.1$, $\tau = 3.0$ ms. Notations and other parameters are the same as in Figure 2.

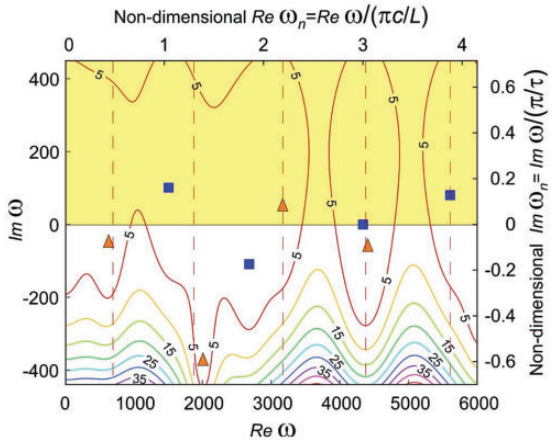

Figure 4. Contour plot of $|g(\omega)|$ for $\tau = 5.0$ ms and $n = 1.1$. Notations and other parameters are the same as in Figure 2.

non-dimensional representation of the real part of frequencies and growth rates of the modes. The real part is non-dimensionalized based on the fundamental modal frequency of acoustic mode ($\pi c/L$ in rad/s), i.e. $Re(\omega_n) = Re(\omega)/(\pi c/L)$. The growth rate is non-dimensionalized by intrinsic instability frequency of the lowest intrinsic mode, i.e. $Im(\omega_n) = Im(\omega)/(\pi/\tau)$. The thin dashed vertical lines indicate the intrinsic mode frequency in the limit of small n, given by equation (8a).

Figure 2 is split into two panels to plot the acoustic and intrinsic modes separately. As the intrinsic modes strongly decay in this limit (when $n = 0.025$), it is more convenient to represent the acoustic and intrinsic modes in two isolated panels. The time lag selected for this figure is 3 ms. The intrinsic modes in the lower panel are equally spaced in this limit of n and their decay rate is too high as predicted by equation (8b) and also evident from Mukherjee et al.[29] When n is increased from 0.025 to 1.1 (as depicted in Figure 3), the first intrinsic and the second acoustic mode become unstable. The decay rates for all other intrinsic modes reduce significantly. As seen in Figure 3, the number of frequencies in the system, indeed, exceeds by far the number of acoustic modes as was also reported by Emmert et al.[14] in their study of a premixed combustor.

When we increase the time lag further from 3 to 5 ms, the intrinsic mode frequency reduces as predicted by equation (8b) (equation (8b) demonstrates $1/\tau$ dependence of intrinsic mode frequency). This is evident from Figure 4. The first acoustic and the third intrinsic modes have become unstable for this time lag. The extensive numerical simulations show that all the intrinsic modes hold the potential to become unstable beyond a certain threshold of n and within certain bands of τ. We will shed some light on this aspect analytically in Section 4. In some cases, the acoustic mode can also become unstable at one of the nearby intrinsic mode frequency in the complex frequency plane. For example, in Figure 3, the second acoustic mode becomes unstable at the second intrinsic mode frequency, 3140 rad/s (in the limit of small n), whereas the second intrinsic mode remains decaying. This is an intrinsic–acoustic mode coupling scenario, a detailed discussion of which lies beyond the scope of the current paper. The acoustic and intrinsic modes are always uncoupled, when n is small (intrinsic modes are very much localized in this limit) and start to feel each other's presence only for sufficiently high n. Once these modes approach the boundary of stability, we apparently have only system modes (neither 'clean acoustic' nor 'clean intrinsic'). Then again, one of the key findings of the paper is that the intrinsic mode (or the coupled-acoustic mode) becomes unstable at $\omega^i = (2m^i + 1)\pi/\tau + m\pi/\tau$ (where $m = 0, +1, -1$) (as will be shown in Section 4.1), whereas the conventional acoustic mode attains instability at $\omega_0^a = m^a(\pi c/L)$. Hence, it is indeed possible to track down the identities of these modes based on their instability frequencies.

Thus, we have shown a set of contour plots for an open–open combustor for different time lags which give a compact visual representation of stable/unstable modes behaviour on the complex frequency plane. The increase of n reduces the decay rate of intrinsic modes, whereas the increase of τ reduces the intrinsic mode frequencies. All the intrinsic modes show a tendency to become unstable beyond a certain threshold value of n and for some τ intrinsic mode can also couple to one of the acoustic modes in their close vicinity in the complex frequency plane. All of these results are consistent with explanations found from Mukherjee et al.[29] and Mukherjee and Shrira,[21] as well.

3.2. Intrinsic mode as the driver of combustion instability

Under certain conditions in an open–open combustor, the intrinsic mode can be unstable, while all the acoustic modes decay simultaneously (or do not grow), thus being the only mechanism of the combustion instability.

Figure 5(a) and (b) illustrates two such cases using contour plots of $|g(\omega)|$. In Figure 5(a), the flame is at $x_q = L/2$. We see that for $n = 2.1$, the first three intrinsic modes are unstable, whereas the acoustic modes remain on the neutral curve of stability, just like they do when $n = 0$. Another example is shown in Figure 5(b), where flame resides at $x_q = 0.20\,\text{m}$. We find that for $n = 1.0$, the first intrinsic mode is unstable, whereas all other modes (acoustic/intrinsic) are either decaying or are on the neutral curve. These two scenarios are examples when intrinsic mode, instead of an acoustic mode, drives the combustion instability. In general, the intrinsic modes attain dominance in the context of combustion instability when all the acoustic modes decay (a) due to negative Rayleigh index or (b) due to increased acoustic losses from the end of the combustor.[15] We can also have a scenario when both acoustic and intrinsic modes can become unstable simultaneously.[37]

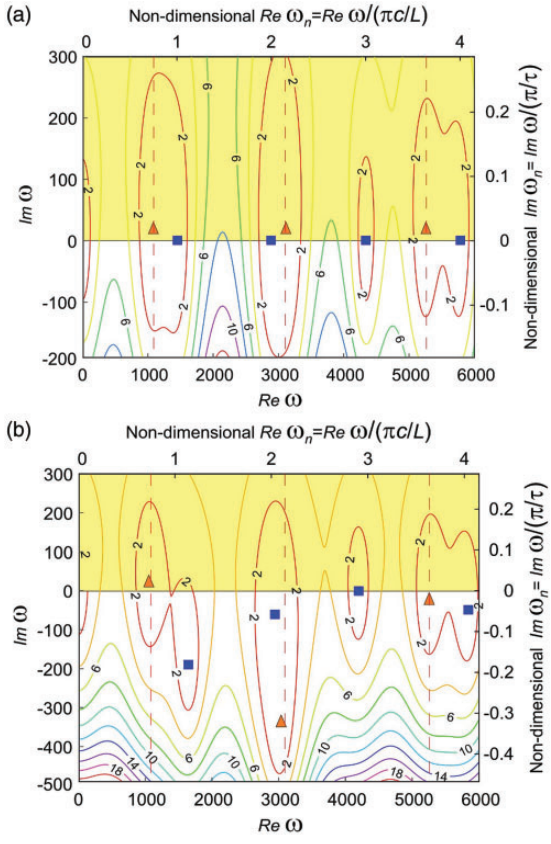

Figure 5. Contour plot of $|g(\omega)|$ for (a) $\tau = 3.0$ ms, $n = 2.1$, $x_q = L/2$ and (b) $\tau = 3.0$ ms, $n = 1.0$, $x_q = 0.20\,\text{m}$. Notation and other parameters are the same as in Figure 2.

An important aspect can be pointed out in this regard. Equation (7) (valid for no cross-section and temperature jumps across the flame) shows decoupling of intrinsic and acoustic modes at $x_q = L/2$. The acoustic modes are given as $\sin(kL) = 0$, whereas the intrinsic mode follow the governing equation: $2 + ne^{i\omega\tau} = 0$. This decoupling holds if the effect of cross-section jump is taken into account, as well. Hence, in the middle of the open–open combustor, acoustic and intrinsic mode stop influencing each other, when we neglect temperature jump.

4. Intrinsic flame instability: Neutral curves and growth rates

In the previous section, we came across the fact that in the limit of small n the flame intrinsic modes decay strongly. However, as we increase n, the decay rate decreases and at some threshold value of n the intrinsic mode becomes unstable. In this section, we find analytically the intrinsic mode incipient instability frequency, the threshold of n for instability and growth rate for flame intrinsic modes. In Section 4.1, we find out the intrinsic mode incipient instability frequency at the neutral curve. Then, in Section 4.2, we obtain the exact threshold value of n for intrinsic mode instability and find the neutral curve in the $n-\tau$ parameter space. Finally, in Section 4.3, we evaluate the linear growth/decay rates near the neutral curve.

4.1. Decoupling on the neutral curve

Here, we will find the incipient instability frequency, i.e. the frequency of the intrinsic mode at the threshold of instability. Let ω_c^i be the discrepancy between the eigenfrequencies ω^i and ω_0^i, the small n prediction given by the real part of equation (8a). Thus, for any n, $Re(\omega^i) = \omega_0^i + \omega_c^i$, where superscript i denotes the intrinsic modes. For any value of n the intrinsic mode frequency ω can be written as $\omega^i = Re(\omega^i) + iIm(\omega^i)$ or $\omega^i = (\omega_0^i + \omega_c^i) + iIm(\omega^i)$. We make use of this expression of ω^i in the dispersion relation (5), then the complete dispersion relation (5) attains the following form

$$\begin{aligned}&(\alpha+1)\sin\{(\omega_0^i+\omega_c^i+iIm(\omega^i))\beta_1\}\\&+(\alpha-1)\sin\{(\omega_0^i+\omega_c^i+iIm(\omega^i))\beta_2\}\\&+2ne^{i(\omega_0^i+\omega_c^i+iIm(\omega^i))\tau}\cos\{(\omega_0^i+\omega_c^i+iIm(\omega^i))x_q/c_1\}\\&\times\sin\{(\omega_0^i+\omega_c^i+iIm(\omega^i))(x_q-L)/c_2\}=0\end{aligned}\qquad(9)$$

where α, β_1 and β_2 are given as

$$\alpha = \left(\frac{S_2}{S_1}\right)\left(\frac{\rho_1 c_1}{\rho_2 c_2}\right),\ \beta_1 = x_q\left(\frac{1}{c_2} - \frac{1}{c_1}\right) - \frac{L}{c_2} \text{ and}$$
$$\beta_2 = \frac{L}{c_2} - x_q\left(\frac{1}{c_1} + \frac{1}{c_2}\right) \tag{10}$$

We make use of the identity, $e^{i\omega_0^i \tau} = -1$ based on equation (8a) and simplify equation (9) further. By definition, $Im(\omega^i)$ is equal to zero for the threshold value of n, i.e. $Im(\omega^i) = 0$ at $n = n_{th}^i$. This specifies the neutral curve. By equating the real part of equation (9) to zero, it can be shown that

$$2in_{th}^i \sin(\omega_c^i \tau)\cos(k_1 x_q)\sin(k_2(x_q - L)) = 0 \tag{11}$$

and thus similar to the case of the closed–open combustor we have decoupling of intrinsic mode frequency on the neutral curve, that is, on the neutral curve the intrinsic mode incipient instability frequency is completely independent of all the parameters of the combustor we take into account in our model (the length, the flame location, cross-section jump and temperature jump) except the time lag τ; and thus $\omega_c^i = m\pi/\tau$, where $m = 0, \pm 1$. The decoupling phenomenon (or the factorization of the dispersion relation) was first reported by Mukherjee and Shrira[21] for a closed–open combustor. This prompts an obvious question: For how many different types of end conditions of the combustor, this kind of decoupling of intrinsic instability frequency from the combustor parameters on the neutral curve takes place? The question can be answered with the help of general dispersion relation when $R_1(0)$ and $R_2(L)$ are retained in the original form in equations (1) and (2)

$$\begin{aligned}&(1+\alpha)\left\{e^{i\omega\beta_1} - R_1(0)R_2(L)e^{-i\omega\beta_1}\right\}\\ &+(1-\alpha)\left\{R_2(L)e^{i\omega\beta_2} - R_1(0)e^{-i\omega\beta_2}\right\} + ne^{i\omega\tau}\left\{e^{i\omega\beta_1}\right.\\ &\left.+R_2(L)e^{i\omega\beta_2} - R_1(0)e^{-i\omega\beta_2} - R_1(0)R_2(L)e^{-i\omega\beta_1}\right\} = 0\end{aligned} \tag{12}$$

where α, β_1 and β_2 are given by equation (10). Making use of $\omega^i = (\omega_0^i + \omega_c^i) + iIm(\omega^i)$, the exponential terms in equation (12) can be expanded as

$$\begin{aligned}e^{i\omega\beta_1} &= e^{i\left(\omega_0^i + \omega_c^i + i\mathrm{Im}(\omega^i)\right)\beta_1}\\ &= e^{-\mathrm{Im}(\omega^i)\beta_1}\left\{\cos\left(\left(\omega_0^i + \omega_c^i\right)\beta_1\right)\right.\\ &\quad\left.+i\sin\left(\left(\omega_0^i + \omega_c^i\right)\beta_1\right)\right\}\end{aligned}$$

The resultant equation can be further simplified at the neutral curve. The real part of equation (12) at the neutral curve can be written as

$$\begin{aligned}&(1+\alpha)(1 - R_1(0)R_2(L))\cos(\omega^i\beta_1)\\ &+(1-\alpha)(R_2(L) - R_1(0))\cos(\omega^i\beta_2)\\ &-n_{th}^i\left[\begin{array}{l}\cos(\omega_c^i\tau)\left\{(1 - R_1(0)R_2(L))\cos(\omega^i\beta_1)\right.\\ \quad\left.+(R_2(L) - R_1(0))\cos(\omega^i\beta_2)\right\}\\ \quad-\sin(\omega_c^i\tau)\left\{(1 + R_1(0)R_2(L))\sin(\omega^i\beta_1)\right.\\ \quad\left.+(R_2(L) + R_1(0))\sin(\omega^i\beta_2)\right\}\end{array}\right] = 0\end{aligned} \tag{12a}$$

And the imaginary part of equation (12) can be written as

$$\begin{aligned}&(1+\alpha)(1 + R_1(0)R_2(L))\sin(\omega^i\beta_1)\\ &+(1-\alpha)(R_2(L) + R_1(0))\sin(\omega^i\beta_2)\\ &-n_{th}^i\left[\begin{array}{l}\cos(\omega_c^i\tau)\left\{(1 + R_1(0)R_2(L))\sin(\omega^i\beta_1)\right.\\ \quad\left.+(R_2(L) + R_1(0))\sin(\omega^i\beta_2)\right\}\\ \quad+\sin(\omega_c^i\tau)\left\{(1 - R_1(0)R_2(L))\cos(\omega^i\beta_1)\right.\\ \quad\left.+(R_2(L) - R_1(0))\cos(\omega^i\beta_2)\right\}\end{array}\right] = 0\end{aligned} \tag{12b}$$

At present, there is no general approach allowing us to solve equations (12a) and (12b) apart from the numerics. However, under some restrictions on $R_1(0)$ and $R_2(L)$ these two equations can be solved analytically. One of the options, found and used in Mukherjee and Shrira,[21] is the case of a closed–open combustor (i.e. $R_1(0) = 1$ and $R_2(L) = -1$), where equation (12b) manifest factorization on the neutral curve

$$2in_{th}^i \sin(\omega_c^i \tau)\sin(k_1 x_q)\sin(k_2(x_q - L)) = 0$$

Another option is exploited in the current paper, where for open–open boundary conditions ($R_1(0) = -1$ and $R_2(L) = -1$) equation (12a) factorizes on the neutral curve. The only other case where factorization occurs is when both ends of the combustor are closed, that is $R_1(0) = 1$ and $R_2(L) = 1$. This particular scenario is of less practical interest for the present design of combustors, nonetheless, should not be neglected as there might be possible applications of this case in other fields of interest. We will, however, refrain from analytical study of this case in the present work. In general, for the decoupling to happen, except one term containing $\sin(\omega_c^i\tau)$ or $\cos(\omega_c^i\tau)$, other terms need to vanish, in either equation (12a) or (12b).

Thus, we get only certain special combinations of $R_1(0)$ and $R_2(L)$ for which multiple multipliers containing $R_1(0)$ and $R_2(L)$ terms in equation (12a) or (12b) vanish. These special combinations are:

(i) $R_1(0) = 1,\ R_2(L) = -1$ (or, $R_1(0) = -1, R_2(L) = 1$),

(ii) $R_1(0) = -1,\ R_2(L) = -1$ and,
(iii) $R_1(0) = 1,\ R_2(L) = 1$

Any other combinations of non-ideal reflection coefficients (including the ones with imaginary parts) prohibit decoupling on the neutral curve. In the current paper, we concentrate only on the case (ii), i.e. on a combustor with ideal open–open boundary conditions.

4.2. The threshold in n for intrinsic instability: Exact solution for the neutral curve

In this section, we derive the exact solution for the threshold in n (n^i_{th}) for the intrinsic mode to become unstable on the $n-\tau$ plane. For each intrinsic mode, we find the neutral curves, i.e. the boundaries of the stability domains on the $n-\tau$ plane.

Making use of the identity, $e^{i\omega^i_0\tau} = -1$ based on equation (8a), the imaginary part of equation (9) on the neutral curve immediately yields us the threshold n^i_{th}

$$n^i_{th} = \frac{\left\{\begin{array}{l}(\alpha+1)\sin\{(\omega^i_0+\omega^i_c)\beta_1\} \\ \quad +(\alpha-1)\sin\{(\omega^i_0+\omega^i_c)\beta_2\}\end{array}\right\}}{2\cos(\omega^i_c\tau)\cos(k_1x_q)\sin\{k_2(x_q-L)\}} \tag{13}$$

where α, β_1 and β_2 are provided by equation (10). First, we examine a special case: $x_q = L/2$, with uniform cross-section and temperature, for which expression (13) can be significantly simplified. For the segment of the neutral curve corresponding to $\omega^i_c\tau = 0$, we find

$$n^i_{th,(0)} = 2 \tag{14a}$$

and for the segments of the neutral curve corresponding to $\omega^i_c\tau = \pi$ and $\omega^i_c\tau = -\pi$ the expressions for n^i_{th} take the form

$$n^i_{th,(\pi)} = -2, \text{ and} \tag{14b}$$

$$n^i_{th,(-\pi)} = -2 \tag{14c}$$

Thus, it is clear that when the flame is located in the middle of the open–open combustor with no temperature and cross-section jump, the threshold of n is constant ($n^i_{th} = 2$) on the neutral curve segment $\omega^i_c\tau = 0$; the threshold is exactly the same as the one found in Hoeijmakers et al.[10] for an anechoic chamber. At this particular flame location, the threshold in n is negative (and therefore unphysical) on the neutral curve segments $\omega^i_c\tau = \pi$ and $\omega^i_c\tau = -\pi$ as per equations (14b) and (14c). Equation (13) stipulates that the threshold of n is 1, when $x_q = 0$ on the neutral curve segment $\omega^i_c\tau = 0$ and -1 on the neutral curve segments $\omega^i_c\tau = \pi$ and $\omega^i_c\tau = -\pi$. Thus, the threshold in n increases as the flame is moved from the flame location $x_q = 0$ to $x_q = L/2$. This is indeed a general trend and it will be shown in the subsequent sections that as we move the flame location from $x_q = 0$ to $x_q = L$, the value of the n-threshold increases.

4.2.1. The neutral curve for a single intrinsic mode on the $n-\tau$ plane. Figure 6(a) shows a sample neutral curve

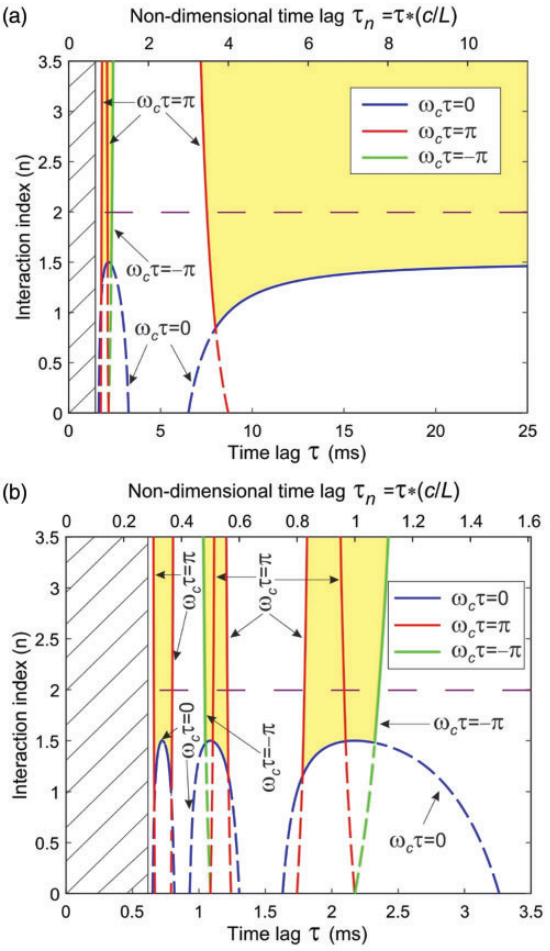

Figure 6. (a) Neutral curve and instability domain (marked in yellow online) on the $n-\tau$ plane for the second intrinsic mode ($m^i = 1$) of an open–open combustor when $x_q = L/3$ and there is no temperature and cross-section jump ($c_1 = c_2 = c = 345$ m/s). As per equation (10), α, β_1 and β_2 are: $\alpha = 1$, $\beta_1 = -L/c = -2.17 \times 10^{-3}$ s and $\beta_2 = L/3c = 0.72 \times 10^{-3}$ s. The segments $\omega^i_c\tau = 0$, $\omega^i_c\tau = \pi$ and $\omega^i_c\tau = -\pi$ of the neutral curve are indicated by arrows (blue, red and green online), respectively. (b) is the same as (a), but extended to show more of the domains with multiple instability islands narrowing with decrease of τ. The dashed lines show their continuations which are also exact solutions of equation (13). We interpret them as neutral curves for acoustic modes coupled to the intrinsic mode. Hatched area indicates the domain with multiple instability islands narrowing with the decrease of τ. The dashed (purple online) horizontal line shows the threshold for an infinite tube: $n^i_{th} = (S_2/S_1)(\rho_1/\rho_2)(c_1/c_2) + 1$.[10] Other parameters are the same as in Figure 2.

(for the second intrinsic mode) of an open–open combustor, when the flame is situated at $x_q = L/3$. The temperature and cross-section are assumed to be uniform and thus $c_1 = c_2 = c = 345\,\text{m/s}$. In all subsequent plots of the neutral curves, in parallel with the dimensional time lag τ, we also use a non-dimensional time lag, $\tau_n = \tau c/L$, employing the natural acoustic mode timescale L/c, where c is the sound speed in the absence of temperature jump. When the fundamental frequencies of acoustic mode and the intrinsic mode are the same, i.e. $\pi/\tau = \pi c/L$, this will correspond to $\tau_n = 1$. The solid lines indicate intrinsic modes and we interpret the dashed lines as the coupled-acoustic modes. The lightly shaded area (yellow online) represents the instability domain for the chosen (second) intrinsic mode. Hatched area indicates the domain with multiple instability islands narrowing with the decrease of τ.

Each neutral loop is a combination of neutral segments $\omega_c^i\tau = 0$, $\omega_c^i\tau = \pi$ and $\omega_c^i\tau = -\pi$, except the loop on the extreme right, which is created by a combination of $\omega_c^i\tau = 0$ and $\omega_c^i\tau = \pi$ (the segment corresponding to $\omega_c^i\tau = -\pi$ does not feature in this loop). Note that the n-threshold saturates for higher time lags, making intrinsic instability possible for any mode for large τ. Indeed, in the case of open–open end conditions, the saturated values of n-threshold can be obtained from equation (13) under the assumption of large time lag. With the assumption that $\sin(\gamma) \approx \gamma$ and $\cos(\gamma) \approx 1$, for small γ, the saturated value of n-threshold comes out to be

$$n_{th}^i = \frac{[(\alpha+1)\beta_1 + (\alpha-1)\beta_2]c_2}{2(x_q - L)} \tag{15}$$

It can be further shown from equation (15) that the saturated value of n-threshold increases as x_q increases. In other words, the boundary of stability moves up, as we increase x_q, indicating that the lower values of x_q are critical from intrinsic instability perspective.

Figure 6(b) is an extension of Figure 6(a) showing that the neutral loops on the left of the neutral curve are a repetitive structure, indeed. In Figure 6(a), we have shown only two neutral loops, whereas in Figure 6(b) we have shown three neutral loops. It is obvious that there are an infinite number of smaller neutral loops on the left of these three loops in Figure 6(b). This infinite number of closely spaced loops is hidden by hatched lines. All the subsequent discussions will be mainly focused on the neutral loop existing on the extreme right. The dashed horizontal line (purple online) in Figure 6 shows the threshold for an infinite tube according to Hoeijmakers et al.[10] For an infinite tube, the threshold in n can be obtained by equating the growth/decay rate to zero in equation (8a). In our notations, the expression for the threshold can be expressed as $n_{th}^i = (S_2/S_1)(\rho_1/\rho_2)(c_1/c_2) + 1$. In Figure 6, $n_{th}^i = 2$ for the uniform tube, i.e. for $S_2/S_1 = 1$, $\rho_1/\rho_2 = 1$ and $c_1/c_2 = 1$. The figure illustrates that for an open–open combustor n_{th}^i can be substantially smaller, as compared to an infinite tube, meaning that in an open–open combustor, the intrinsic modes can become unstable at a much lower value of n. This observation is in line with the similar one made by Mukherjee and Shrira[21] for closed–open combustors. The analytical solution (13) for neutral curve is exact, a numerical validation of which can be found in Mukherjee[38] and also in Mukherjee and Shrira[21] for closed–open combustors (with and without temperature and cross-section jump).

We note that every small or large loop on the neutral curve is a result of intrinsic–acoustic mode coupling. Indeed, the neutral curve segments $\omega_c^i\tau = \pi$ and $\omega_c^i\tau = -\pi$ originate due to this coupling. Figure 6(a) and (b) makes it evident that near the intersection of neutral curve segments $\omega_c^i\tau = 0$, $\omega_c^i\tau = \pi$, and also $\omega_c^i\tau = 0$, $\omega_c^i\tau = -\pi$, we observe two solutions for the same time lag. The first solution corresponds to intrinsic mode, whereas the second solution (which is also a solution of equation (13)) represents a coupled-acoustic mode. We refer this as the domain of coupling on the neutral curve. We witness single uncoupled solution for the intrinsic mode corresponding to $\omega_c^i\tau = 0$, between these two intersection points. The coupled modes invariably tend to change their identity in the vicinity of intersections of the neutral curve segments, an observation reported by Mukherjee and Shrira.[21] In the absence of coupling, intrinsic mode attains instability at a frequency corresponding to $\omega_c^i\tau = 0$, whereas the coupling induces a frequency shift of $\pm\pi/\tau$ to one of the nearby acoustic modes. A detailed discussion of coupling will be reported elsewhere.

4.2.2. The neutral curve for multiple intrinsic modes on the $n-\tau$ plane. Figure 7 shows a multi-mode instability map where we can just overlap the stability plots for multiple intrinsic modes and get an idea about the overall instability domain.

We indicate the first ($m^i = 0$), second ($m^i = 1$) and third ($m^i = 2$) intrinsic modes using arrows (red, blue and magenta online, respectively). The figure illustrates that as the mode number m^i increases, (a) the neutral curve main loop shifts to the right; (b) the span of the islands of instability on the left increases; (c) the segments corresponding to $\omega_c^i\tau = \pi$ and $\omega_c^i\tau = -\pi$ become less steep for higher modes. Another important aspect is the domain marked by (vii) (light yellow online) in the asymptotic limit of large τ. This domain represents the common instability domain for the first three intrinsic modes. For an open–open combustor, the intrinsic modes are potentially unstable even for the large

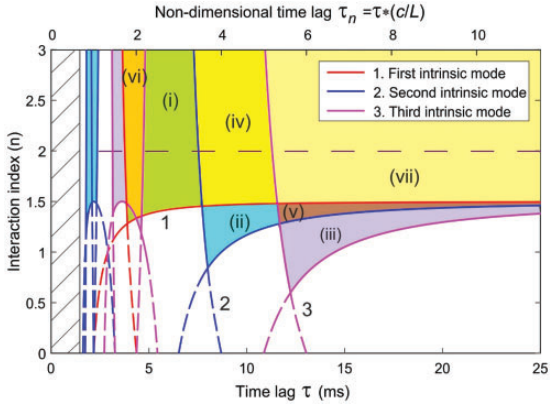

Figure 7. The neutral curves and instability domain on the $n-\tau$ plane for the first ($m^i=0$), second ($m^i=1$) and third ($m^i=2$) intrinsic modes of an open–open combustor when $x_q = L/3$ and there is no temperature and cross-section jump ($c_1 = c_2 = c = 345$ m/s). (1) (red online), (2) (blue online) and (3) (magenta online) represents neutral curves for first, second and third intrinsic modes, respectively. The common domain of instability for the first and second modes is (iv) (yellow online), for the second and third intrinsic modes, it is (v) (brown online) and for first and third intrinsic modes is (vi) (gold online). (vii) (light yellow online) indicates the domain where all three modes are unstable. (i) (lime online), (ii) (light turquoise online) and (iii) (lavender online) indicate the non-overlapping domains of instability for the first, second and third intrinsic modes, respectively. The notation and parameters are the same as in Figure 6.

time lag. The threshold of n also tends to go down for higher order modes in the asymptotic limit of large τ and the corresponding n^i_{th} can be calculated using formula (15). Moreover, Figures 6 and 7 suggest that the characteristic values of n^i_{th} are smaller, as compared to the threshold values of n as reported by Hoeijmakers et al.[10] derived based on the scattering matrix of the flame alone, completely independent of the acoustic boundary conditions. Hence, the intrinsic modes can become unstable at a much lower value of n than the theoretical prediction for an infinite tube. Figure 7 also confirms that beyond certain time lag, the first intrinsic mode is always unstable. The same is true for other intrinsic modes, as well. Crucially, the first intrinsic mode provides the upper bound of the stability domain. In other words, any point on the $n-\tau$ plane that is above this upper bound is guaranteed to be unstable for at least one or multiple intrinsic modes. For a closed–open combustor, the geometry of the instability domain is very different, a detailed discussion on the upper and lower bound of intrinsic mode stability envelope can be found in Mukherjee and Shrira.[21] Indeed, the domain of instabilities shown here proves to be qualitatively different from that of closed–open combustors: there is a threshold in τ above which many intrinsic modes are unstable provided n exceeds a certain threshold (given by equation (15)). This is in sharp contrast with closed–open systems where for large τ the instability domain due to large neutral loop can overlap only for maximum two intrinsic modes. Having said that we have not noticed any discernible difference between the small neutral loops on the left for an open–open system and that of a closed–open system. A detailed investigation of these small neutral loops should be a subject of a dedicated study.

4.2.3. Numerical explanation of modal stability/instability of intrinsic modes on the complex frequency plane. A number of obvious questions regarding intrinsic mode instability arise while studying Figures 6 and 7 of the current paper and also, Figure 9 of Mukherjee and Shrira.[21] The first obvious question is the 'evolution'/visualization of n^i_{th} on the complex frequency plane per se, which was briefly touched in Section 3 and will be discussed in more detail here. Few numerical examples will be considered where by gradually varying n at a fixed τ, we will elucidate the trajectory of the frequencies and growth/decay rate of intrinsic modes on the complex frequency plane. The next natural question is related to the scenario when, for certain τ, an intrinsic mode manifests coupling/no-coupling due to alteration of the acoustic boundary condition from closed to open and vice versa. The features of two solutions co-existing at the point of intersection of the neutral curve segments will be discussed here, as well. Also, it is a matter of interest – the stability features of the intrinsic modes within the domain of $n-\tau$ plane where no n^i_{th} exists as per Figure 6. All of these points will be scrutinized using Figures 8 to 10.

Figure 8 illustrates the loci of the intrinsic and the coupled-acoustic modes for the closed–open and open–open combustors for two different time lags, $\tau = 11$ ms and 11.5 ms. Panels (b) and (d) are mere reproduction of panels (a) and (c) in order to elucidate the fact that intrinsic mode frequencies are independent of the combustor environment variables (excluding τ) in the limit of small n. The figure presents the stability features of the second intrinsic mode ($m^i=1$). It can be seen that due to gradual increase of n, the modes (both coupled-acoustic and intrinsic) tends to cross the neutral line for this case. However, there are two major differences in the features of the coupled-acoustic and intrinsic modes (for closed–open combustor);

(i) The coupled-acoustic mode, in both panels (a) and (c), initially decays as n increases and then after some n (this n is not a topic of investigation of this paper) the loci change their trajectory to make the coupled-acoustic mode unstable. In contrast, the intrinsic mode decay rate monotonically

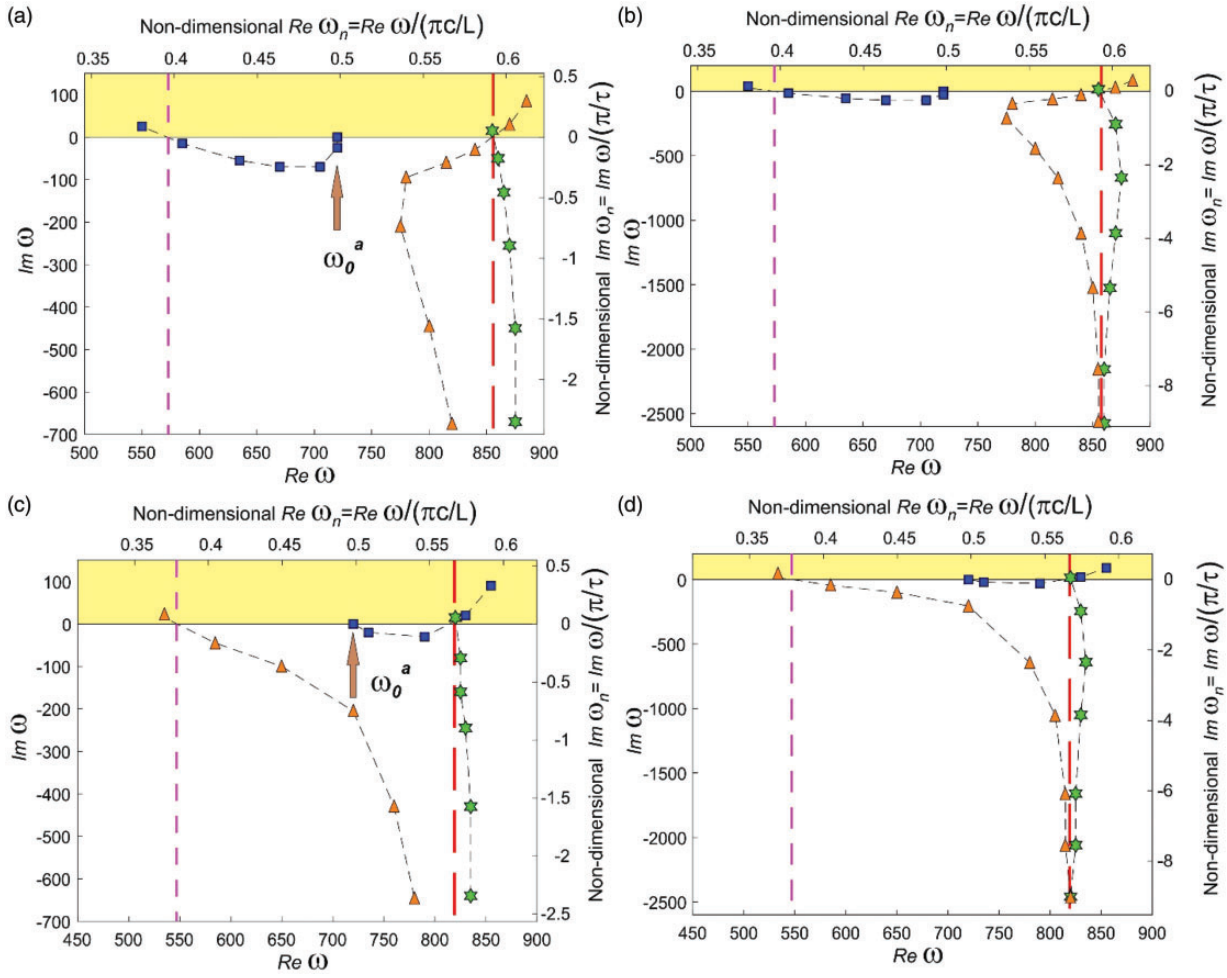

Figure 8. Loci of the intrinsic and coupled-acoustic modes on the complex frequency plane for closed–open and open–open combustors with uniform temperature and cross-section. The triangle (orange online) and square (blue online) dots represent numerical solution (equation (10) from Mukherjee and Shrira[21]) of the intrinsic and coupled-acoustic modes for closed–open system (for $x_q = 0.375$ m, $m^a = 0$, $m^i = 1$). The star (green online) dots indicate the numerical solution (5) of the intrinsic mode for open–open system (for $x_q = 0.25$ m, $m^i = 1$). The loci have been marked by thin dotted black line to facilitate easy comprehension. Panels (a) and (c) indicate solutions for $\tau = 11$ ms and 11.5 ms, respectively, when n is varied from 0.001 to 1.5. Panels (b) and (d) are reproduction of the diagram in panels (a) and (c), however, on a different scale capturing frequencies/growth rates at small n (n changes from 10^{-12} to 1.5), to establish the fact that the intrinsic mode frequencies are independent of the combustor environment variables (barring τ) in the limit of small n. Lightly shaded region (yellow online) is the domain of instability. The arrow indicates the frequency of acoustic mode ($\omega_0^a = (2m^a + 1)(\pi c/2L)$, $m^a = 0,1,2,3,\ldots$) of the closed–open combustor in the absence of flame. Thick dashed (red online) and thin dashed (magenta online) vertical lines indicate the modal frequencies corresponding to $\omega_c^i\tau = 0$ and $\omega_c^i\tau = -\pi$ neutral segments, respectively.

reduces as n gets ramped up, till the mode crosses the neutral line of instability.

(ii) The coupled-acoustic and intrinsic modes do not get unstable at the same frequency. Panel (a) (also panel (b)) suggests that the intrinsic mode attains instability at a frequency corresponding to $\omega_c^i\tau = 0$, whereas the coupled-acoustic mode attains instability at a frequency corresponding to $\omega_c^i\tau = -\pi$. Exactly opposite trend is visible in panel (c) (and also panel (d)), where the coupled-acoustic mode attains instability at a frequency corresponding to $\omega_c^i\tau = 0$, whereas the intrinsic mode attains instability at a frequency corresponding to $\omega_c^i\tau = -\pi$.

Needless to say that for the open–open combustor, at these two time lags, only intrinsic mode becomes unstable (see panels (a) to (d)) at a frequency corresponding to $\omega_c^i\tau = 0$ and hence on the neutral curve we find only one solution (see Figure 6). For the closed–open combustor, on the contrary, at these two time lags both intrinsic and coupled-acoustic mode becomes

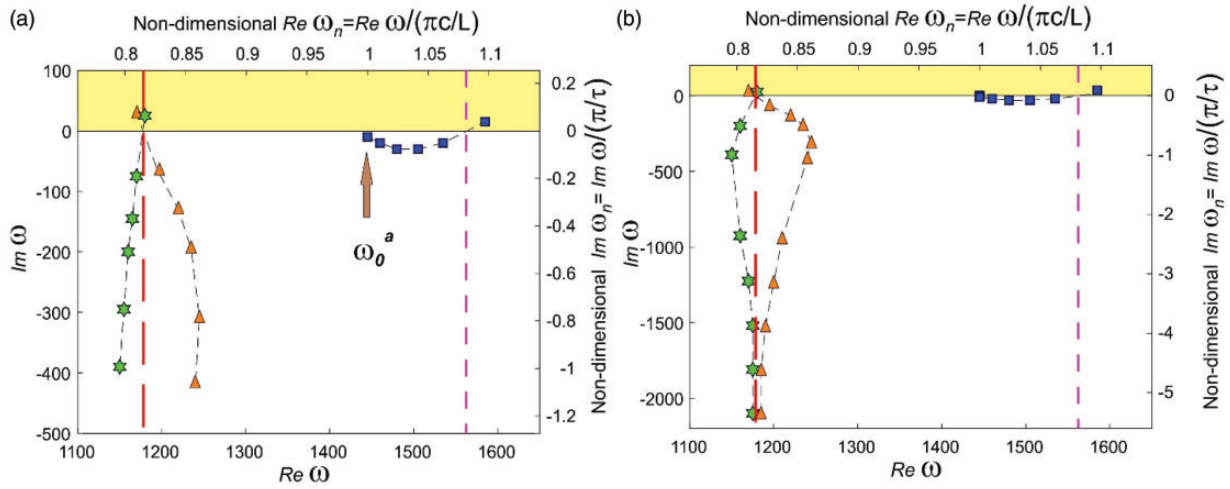

Figure 9. Loci of the intrinsic and coupled-acoustic modes on the complex frequency plane for closed–open and open–open combustors with uniform temperature and cross-section at $\tau = 8$ ms (also shown to be the point of intersection of neutral curve segments $\omega_c^i\tau = 0$ and $\omega_c^i\tau = \pi$ as per Figure 6). The triangle (orange online) and square (blue online) dots represent numerical solution (5) of the intrinsic and coupled-acoustic modes for open–open system (for $x_q = 0.25$ m, $m^a = 1$, $m^i = 1$). The star (green online) dots indicate the numerical solution (equation (10) from Mukherjee and Shrira[21]) of the intrinsic mode for closed–open system (for $x_q = 0.375$ m, $m^i = 1$). Panel (a) indicates solutions when n is varied from 0.05 to 1.1. Panel (b) is the same as panel (a), however, on a different scale, as n is varied from 10^{-7} to 1.1. The arrow indicates the frequency of acoustic mode ($\omega_0^a = m^a(\pi c/L)$, $m^a = 1,2,3,\ldots$) of the open–open combustor in the absence of flame. Thick dashed (red online) and thin dashed (magenta online) vertical lines indicate the modal frequencies corresponding to $\omega_c^i\tau = 0$ and $\omega_c^i\tau = \pi$ neutral segments, respectively. Other notations are the same as in Figure 8.

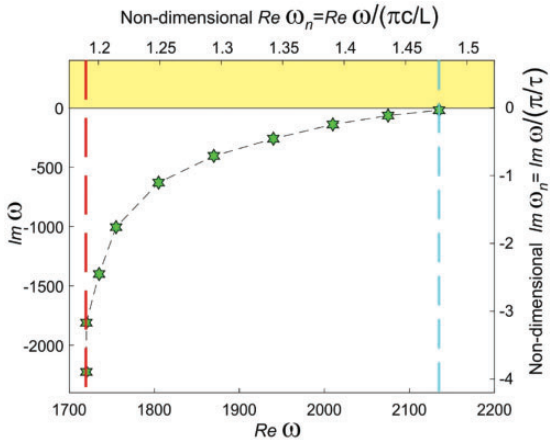

Figure 10. Loci of the intrinsic mode on the complex frequency plane for open–open combustors with uniform temperature and cross-section at τ=5.5 ms (also shown to be the point on the neutral curve where no n_{th}^i exists as per Figure 6), while n varies from 10^{-5} to 10^3. The star (green online) dots indicate the numerical solution (equation (5)) of the intrinsic mode (for x_q=0.25 m, $m^i = 1$). Thick dashed (red online) and thin dashed (cyan online) vertical lines indicate the modal frequencies corresponding to $\omega_c^i\tau = 0$ and $\cos(k_1 x_q) = 0$ as per equation (11), respectively. Other notations are the same as in Figure 8.

unstable (see panels (a) to (d)) and hence on the neutral curve we witness two solutions (see Figure 9 in the literature[21]). Moreover, we can see in panels (a) to (d) that when two solutions exist for the same time lag on the neutral curve (in this case for closed–open combustor), the intrinsic mode frequency drifts significantly from the frequency prescribed by the $\omega_c^i\tau = 0$ line, in particular, near the boundary of instability. This drift is marginal when we have only one solution for intrinsic mode for a time lag on the neutral curve (in this case for open–open combustor). The n_{th}^i corresponding to the mode on the neutral curve segment $\omega_c^i\tau = 0$ is much lower than that on the neutral curve segment $\omega_c^i\tau = -\pi$ (as can be seen from Figure 6 for $\tau = 11$ ms and 11.5 ms), which is also evident from the panels (a) to (d), indicating much higher growth rate of the mode corresponding to segment $\omega_c^i\tau = 0$ than that of $\omega_c^i\tau = -\pi$, for the same n.

Another example provided by Figure 9 illustrates the case when we have two solutions (coupled-acoustic and intrinsic) for the same time lag on the neutral curve at the point where the neutral curve segments intersect, that is $\tau = 8$ ms for second intrinsic mode in open–open combustor (as shown in Figure 6). Qualitatively, this figure is not different from Figure 8, as we have two solutions for open–open combustor: (i) the intrinsic mode attaining instability at a frequency corresponding to $\omega_c^i\tau = 0$ and (ii) the coupled-acoustic mode attaining instability at a frequency corresponding to $\omega_c^i\tau = \pi$. However, there is still a salient difference between Figures 8 and 9. Unlike Figure 8, in Figure 9, both the coupled-acoustic and intrinsic modes cross the neutral line at the same n ($n = 0.85$), implying the same n_{th}^i

for two modes; this is the main significance of the neutral curve intersection points. At the same instance, the intrinsic mode for closed–open combustor attains instability at a frequency corresponding to $\omega_c^i\tau = 0$, and hence we find single solution for $\tau = 8$ ms on the neutral curve (see Figure 9 in the literature[21]).

A case study as shown in Figure 10 intends to explain what happens in the domain of the neutral curve where no solution exists. In Section 3, we claimed that the intrinsic modes remain linearly stable for really large n. Figure 10 validates and illustrates this claim. The figure shows that for $\tau = 5.5$ ms, as we increase n to a really large value ($n = 1000$), the intrinsic mode tends to touch the neutral line of stability, but does not cross it. Interestingly, the intrinsic mode stabilizes at a frequency corresponding to $\cos(k_1 x_q) = 0$ as per equation (11). We can see that although we claimed that the feasible solution for the neutral curve follows from $\sin(\omega_c^i\tau) = 0$, as per equation (11), we have two more potential solutions, i.e. $\cos(k_1 x_q) = 0$ and $\sin(k_2(x_q - L)) = 0$, each of them indicating $n_{th}^i \to \infty$ as per equation (13). Thus, whenever an intrinsic mode stabilizes at a frequency corresponding to $\cos(k_1 x_q) = 0$ or $\sin(k_2(x_q - L)) = 0$, we have an infinite n_{th}^i, implying no solution on the neutral curve and thus stability of this mode in the chosen range of parameters.

4.2.4. The reason for the qualitative difference between the neutral curves of the closed–open and open–open combustors. At this point, we can try to delve into the reason why the closed–open and open–open neutral curves have different geometries. From Figure 6 it is easy to see that the neutral curve attains a loop shape in the domain of two solutions ($\omega_c^i\tau = 0$ and $\omega_c^i\tau = \pi$ or $\omega_c^i\tau = 0$ and $\omega_c^i\tau = -\pi$), which is the result of the intrinsic mode's existence in a close proximity to one of the acoustic modes in the complex frequency plane, which eventually results in intrinsic–acoustic mode coupling. In a system devoid of coupling (anechoic systems), we have a straight line on the $n - \tau$ plane as shown by Hoeijmakers et al.[10] and also shown in Figures 6 and 7. Each neutral loop is a manifestation of coupling with particular acoustic modes, but the extreme right (the main) neutral curve loop always finds coupling with the lowest (or first) acoustic mode (because the extreme right neutral loop contains lower intrinsic mode frequencies that can come close to the lowest acoustic mode frequencies only, on the complex frequency plane) and the loops on the subsequent left side finds coupling with the higher order acoustic modes. Let us take two examples to elucidate this aspect further:

(i) In Figure 9 of Mukherjee and Shrira,[21] the extreme right portion of the extreme right neutral loop ($\omega_c^i\tau = 0$) couples with the $m^a = 0$ acoustic mode, in this case ($\pi c/2L$) (we know that in the closed–open system the acoustic modes are $(2m^a + 1)(\pi c/2L)$). The loops on the left couple with the $m^a = 1,2,3,\ldots$ acoustic modes.

(ii) In contrast, in Figure 6 of the current paper, the extreme right portion of the extreme right neutral loop ($\omega_c^i\tau = 0$) tries to couple with the $m^a = 0$ acoustic mode, which is in this case zero (we know that in the open–open system the acoustic modes are $m^a(\pi c/L)$). Because the $m^a = 0$ acoustic mode is non-existent in open–open systems, the corresponding coupling also does not exist, implying that the extreme right $\omega_c^i\tau = 0$ neutral loop fails to bend on the right side and remains open. Hence, we have uncoupled intrinsic mode solution only.

This explains that the observed qualitative difference in closed–open and open–open neutral loop geometries are related to the coupling with $m^a = 0$ acoustic mode frequency, which is boundary condition dependent.

Thus, we have arrived at an explicit analytical expression (13) for the neutral curves on the $n - \tau$ plane for an open–open combustor. For an open–open combustor, the neutral curves for flame intrinsic modes have two qualitatively different regions. The region on the left, i.e. towards smaller values of τ, comprises loops of diminishing (towards smaller) τ widths made of strongly coupled acoustic–intrinsic modes and the region on the right exhibits a single large loop which stretches to infinity in τ. For open–open combustor, the neutral curve has three distinct segments corresponding to $\omega_c^i\tau = 0$, $\omega_c^i\tau = \pi$ and $\omega_c^i\tau = -\pi$ in the $n - \tau$ space except the first intrinsic mode, where the neutral curve segments due to $\omega_c^i\tau = -\pi$ do not exist, since it predicts zero frequency and infinite n_{th}^i as per equation (13). The $\omega_c^i\tau = \pi$ and $\omega_c^i\tau = -\pi$ segments predict higher values of n_{th}^i compared to $\omega_c^i\tau = 0$ segments. These segments become less steep as the mode number m^i increases. For an open–open combustor, we have a domain in the asymptotic limit of large τ on the $n - \tau$ plane, where a really large number of intrinsic modes become linearly unstable. We can also find analytically the locations of the intersection points of the neutral curve segments $\pm\omega_c^i\tau = \pi$ and $\omega_c^i\tau = 0$. But this aspect will not be discussed here.

4.3. Growth rate of intrinsic and coupled-acoustic modes

The growth rate is the next key element that we need to explore in combustion instability. We concentrate on the growth/decay rates near the neutral curve, only. For large deviations away from the neutral curve, the

intrinsic modes either strongly decay and, hence, do not play any role in the dynamics of the system or have too high growth rates, which implies that the adopted linear theory becomes invalid at that point.

We consider a point (n, τ) on the $n-\tau$ plane located close to the neutral curve for a specific mode m^i. The deviation from the neutral curve is denoted by n_1^i, hence $n - n_{th}^i = n_1^i \ll n_{th}^i$. The eigen-frequency in the chosen point (n, τ) differs from its value on the neutral curve ω^i (where $\omega^i = \omega_0^i + \omega_c^i$) for the same τ. This deviation is denoted as ω_1^i. As per numerical observation, close to the neutral curve the real frequency shifts only marginally. Thus, we assume that the real part of ω_1^i is negligibly small compared to its imaginary part and of little interest near the neutral curve. The imaginary part of ω_1^i, on the other hand, represents the growth/decay rate. For any frequency perturbation ω_1^i due to deviation n_1^i near the neutral curve, we can write $n = n_{th}^i + n_1^i,\ \omega = \omega^i + \omega_1^i$

For simplicity, we only consider the first-order term in n_1^i. Higher order corrections in n_1^i can be dealt with in similar manner. We refrain from that task for the time being. Substituting these expressions for n and ω into the original dispersion relation (5) and subtracting the dispersion relation (5) for $\omega = \omega^i$ from the resultant equation, while neglecting higher order terms in ω_1^i in sin and cos function expansion, we obtain a perturbed form of the dispersion relation (5). This perturbed form instantly yields an explicit analytical expression for the growth/decay rate ω_1^i

$$\omega_1^i = \frac{2n_1^i e^{i\omega^i\tau}\cos(\omega^i x_q/c_1)\sin(\omega^i(x_q-L)/c_2)}{-[(\alpha+1)\beta_1\cos(\omega^i\beta_1)+(\alpha-1)\beta_2\cos(\omega^i\beta_2)+\Sigma]} \tag{16}$$

where $\sum$ is

$$\begin{aligned}\sum = 2n_{th}^i e^{i\omega^i\tau}\{&i\tau\cos(\omega^i x_q/c_1)\sin(\omega^i(x_q-L)/c_2)\\ &-(x_q/c_1)\sin(\omega^i x_q/c_1)\sin(\omega^i(x_q-L)/c_2)\\ &+((x_q-L)/c_2)\cos(\omega^i x_q/c_1)\cos(\omega^i(x_q-L)/c_2)\}\end{aligned}$$

while α, β_1 and β_2 are given by equation (10). Through a numerical examination of multiple examples, it has been observed that the real part of ω_1^i is indeed insignificant as was assumed in the beginning of this derivation. Thus, $\omega_1^i \approx Im(\omega_1^i)$ and represents the growth/decay rate. Equation (16) shows dependence on combustor parameters. Note that equation (16) offers growth/decay rate expressions not only for the modes lying on the neutral curve segment $\omega_c^i\tau = 0$ but also for the modes lying on the neutral curve segments $\omega_c^i\tau = \pm\pi$.

Thus, we have found an explicit formula for the intrinsic mode growth/decay rates in the vicinity of the neutral curve on the $n-\tau$ plane, while on the neutral curve we found decoupling of the combustor characteristics and flame location, the growth rate formula has retained dependence on various combustor parameters. For simplicity, we only consider the first-order term in n_1^i. Higher order corrections in n_1^i are straightforward analytical extensions. The range where this growth rate formula is applicable is to be established numerically. Here, we examine the full dispersion relation (5) numerically. We consider the parameters of the test rig at IIT Madras[35]: the length L is 0.75 m, the cross-section S is 0.0016 m^2 (The actual combustor at IIT Madras is closed–open. However, here we use the physical dimensions of the combustor only.). The flame is assumed to be located at $x_q = L/3$. The same parameters were used for plotting all the stability diagrams.

Figure 11 shows a comparison of the analytical prediction of the growth rates given by equation (16) with that of the numerical results for $m^i = 1,\ x_q = L/3$, $\tau = 7$ ms, and the cross-section and temperature jump $(S_2/S_1 = 1.5,\ T_2/T_1 = 2.25)$. Near n_{th}^i, that is near the boundary of stability, analytical and numerical predictions match up quite nicely. However, as we move away from the neutral curve, analytical predictions start to deviate from the numerical results. Beyond this range, modes are either stable or linear theory is not applicable anymore (the linear theory is based on the small growth/decay rate assumption). All these observations hold if the effect of cross-section and temperature jump is taken into consideration. We can, therefore, conclude

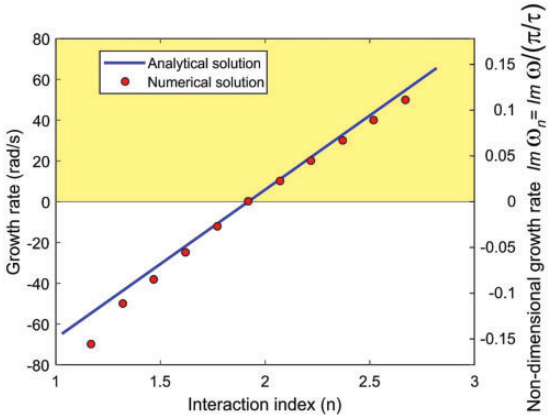

Figure 11. Growth rate for $m^i = 1$, $x_q = L/3$, $\tau = 7$ ms, and the cross-section and temperature jump $(S_2/S_1 = 1.5,\ T_2/T_1 = 2.25)$: comparison of the analytical result (16) and numerical solution of the original dispersion relation (5). The solid line and circles show the analytical and numerical solution, respectively. The instability domain is lightly shaded (yellow online). Dimensional (rad/s), as well as, non-dimensional $(Im(\omega_n) = Im(\omega)/(\pi/\tau))$ scales are used for the growth rate. The other parameters of the system are the same as in Figure 6(a).

that the analytical prediction for the growth rate is in good agreement with the numerical solution in the moderate proximity of n^i_{th}, where it is of most interest. Our approximate solution (16) considers only the leading order term of expansion in n^i_1 (the departure of n from n^i_{th}). This expansion provides a good level of accuracy near the neutral curve for all the cases we have studied so far. If we look for higher accuracy, it is straightforward to consider higher order expansion in n^i_1 in our perturbation equation. Equation (16) has been checked for accuracy for various other time lag values on the neutral curve including the vicinity of intersections of different neutral segments and has been found to work with a good accuracy near the neutral curve.[38]

Hence, we have confirmed that the compact analytical prediction of the linear growth rate (16) works very well for all τ. The growth/decay rate depends on various combustor parameters. A parametric study of the growth rate and neutral curves will be performed in Section 6.

5. Intrinsic instability for combustors with non-ideal open–open boundaries

In reality, it is not necessarily a good approximation to say that the reflection coefficients are equal to ± 1, as it has been assumed so far here and also in the literature.[21] Reflection coefficients are complex, meaning the reflection coefficient has a dissipative and a reactive part associated with it. The energy losses at the ends of the combustor account for the dissipative component in the reflection coefficient. A perfectly rigid or closed end will reflect the incident waves totally, without acoustic losses,[26] meaning the assumption made in Mukherjee and Shrira[21] for the closed end reflection coefficient being $+1$ is a valid one. However, this assumption is not so accurate for the open end. Acoustic radiations from the end of a duct will be impeded by the atmosphere, a phenomenon represented by a parameter called the radiation impedance, which is a complex number for any open duct.[26] For cylindrical ducts and normal acoustic modes, the exact solution for the radiation impedance has been provided by Levine and Schwinger.[39] The exact expression for reflection coefficient of the open end of a circular duct with radius r_0 is given as[26]

$$R = \left(1 - 0.5k^2 r_0^2\right) \exp\left\{i\left(\pi - 1.2\tan^{-1}(kr_0)\right)\right\}$$

Clearly, the reflection coefficient for an open end is nearly unity and the phase angle is slightly less than π, meaning that the coefficient is not exactly -1 as we assumed so far. This assumption is valid only when the non-dimensional number Helmholtz number kr_0 is small. This is, indeed, a low-frequency assumption. The reflection coefficient is a frequency dependent parameter in most of the cases. Besides, it was mentioned in the Introduction that in industrial gas turbine combustors there is a compressor assembly in the upstream and turbine assembly in the downstream, imposing limitations on the ideal open/closed assumption. In this section, we address this issue.

5.1. Instability frequencies and neutral curves

When $R_1(0)$ and $R_2(L)$ are retained in the original form in equations (1) and (2), we derive the general dispersion relation as shown in equation (12). The real and imaginary parts of equation (12) are written as (12a) and (12b) on the neutral curve. Now, we consider a case when the end conditions of the combustor are not perfectly open–open and in that case, we can write the reflection coefficients for the ends as

$$R_1(0) = -1 + \varepsilon_1 r_1, \text{ and} \tag{17a}$$

$$R_2(L) = -1 + \varepsilon_2 r_2 \tag{17b}$$

where ε_1 and ε_2 are two small parameters characterizing smallness of the deviation from the ideal open–open end condition, r_1 and r_2 are order one complex quantities specified by the experimental data. r_1 and r_2 can be written as $r_1 = Re(r_1) + iIm(r_1)$ and $r_2 = Re(r_2) + iIm(r_2)$. Replacing $R_1(0)$ and $R_2(L)$ as per equations (17a) and (17b) and neglecting the higher order terms, equations (12a) and (12b) reduce to the following form on the neutral curve

$$\begin{aligned}
&(1+\alpha)\left[(\varepsilon_1 Re(r_1) + \varepsilon_2 Re(r_2))\cos\left(\omega^i\beta_1\right)\right.\\
&\left.+(\varepsilon_1 Im(r_1) + \varepsilon_2 Im(r_2))\sin\left(\omega^i\beta_1\right)\right]\\
&+(1-\alpha)\left[(\varepsilon_2 Re(r_2) - \varepsilon_1 Re(r_1))\cos\left(\omega^i\beta_2\right)\right.\\
&\left.-(\varepsilon_1 Im(r_1) + \varepsilon_2 Im(r_2))\sin\left(\omega^i\beta_2\right)\right]\\
&-n^i_{th}\left[\begin{array}{l}
\cos\left(\omega^i_c\tau\right)\left\{\begin{array}{l}
(\varepsilon_1 Re(r_1) + \varepsilon_2 Re(r_2))\cos\left(\omega^i\beta_1\right)\\
+(\varepsilon_1 Im(r_1) + \varepsilon_2 Im(r_2))\sin\left(\omega^i\beta_1\right)\\
+(\varepsilon_2 Re(r_2) - \varepsilon_1 Re(r_1))\cos\left(\omega^i\beta_2\right)\\
-(\varepsilon_1 Im(r_1) + \varepsilon_2 Im(r_2))\sin\left(\omega^i\beta_2\right)
\end{array}\right\}\\
+\sin\left(\omega^i_c\tau\right)\left\{\begin{array}{l}
-2\sin\left(\omega^i\beta_1\right) - (\varepsilon_1 Im(r_1)\\
+\varepsilon_2 Im(r_2))\cos\left(\omega^i\beta_1\right)\\
+2\sin\left(\omega^i\beta_2\right) - (\varepsilon_2 Im(r_2)\\
-\varepsilon_1 Im(r_1))\cos\left(\omega^i\beta_2\right)
\end{array}\right\}
\end{array}\right]\\
&=0
\end{aligned} \tag{18a}$$

$$
\begin{aligned}
&(1+\alpha)\left[-2\sin\left(\omega^i\beta_1\right)-\left(\varepsilon_1 Im(r_1)+\varepsilon_2 Im(r_2)\right)\right.\\
&\left.\times\cos\left(\omega^i\beta_1\right)\right]-(1-\alpha)\left[-2\sin\left(\omega^i\beta_2\right)+\left(\varepsilon_2 Im(r_2)\right.\right.\\
&\left.\left.-\varepsilon_1 Im(r_1)\right)\cos\left(\omega^i\beta_2\right)\right]\\
&-n^i_{th}\left[\begin{array}{l}
\cos\left(\omega^i_c\tau\right)\left\{\begin{array}{l}
-2\sin\left(\omega^i\beta_1\right)-\left(\varepsilon_1 Im(r_1)\right.\\
\left.+\varepsilon_2 Im(r_2)\right)\cos\left(\omega^i\beta_1\right)\\
+2\sin\left(\omega^i\beta_2\right)-\left(\varepsilon_2 Im(r_2)\right.\\
\left.-\varepsilon_1 Im(r_1)\right)\cos\left(\omega^i\beta_2\right)
\end{array}\right\}\\
-\sin\left(\omega^i_c\tau\right)\left\{\begin{array}{l}
\left(\varepsilon_1 Re(r_1)+\varepsilon_2 Re(r_2)\right)\cos\left(\omega^i\beta_1\right)\\
+\left(\varepsilon_1 Im(r_1)+\varepsilon_2 Im(r_2)\right)\sin\left(\omega^i\beta_1\right)\\
+\left(\varepsilon_2 Re(r_2)-\varepsilon_1 Re(r_1)\right)\cos\left(\omega^i\beta_2\right)\\
-\left(\varepsilon_1 Im(r_1)+\varepsilon_2 Im(r_2)\right)\sin\left(\omega^i\beta_2\right)
\end{array}\right\}
\end{array}\right]\\
&=0
\end{aligned}
\tag{18b}
$$

Equations (18a) and (18b) provide explicit expressions for n^i_{th}. Equating n^i_{th} from equations (18a) and (18b) leads to the following equation

$$
\begin{aligned}
&\left[\begin{array}{l}
2\left(\sin\left(\omega^i\beta_1\right)-\sin\left(\omega^i\beta_2\right)\right)\\
\left\{(1+\alpha)\sin\left(\omega^i\beta_1\right)-(1-\alpha)\sin\left(\omega^i\beta_2\right)\right\}\\
+\varepsilon_1 Im(r_1)\left\{(1+\alpha)\sin\left(2\omega^i\beta_1\right)\right.\\
\left.+(1-\alpha)\sin\left(2\omega^i\beta_2\right)-2\sin\left(\omega^i(\beta_1+\beta_2)\right)\right\}\\
+\varepsilon_2 Im(r_2)\left\{(1+\alpha)\sin\left(2\omega^i\beta_1\right)\right.\\
\left.+(1-\alpha)\sin\left(2\omega^i\beta_2\right)+2\sin\left(\omega^i(\beta_1-\beta_2)\right)\right\}
\end{array}\right]\sin\left(\omega^i_c\tau\right)\\
&=2\alpha\left[\begin{array}{l}
\varepsilon_1 Re(r_1)\sin\left(\omega^i(\beta_2-\beta_1)\right)\\
+\varepsilon_2 Re(r_2)\sin\left(\omega^i(\beta_1+\beta_2)\right)
\end{array}\right]\cos\left(\omega^i_c\tau\right)
\end{aligned}
\tag{19}
$$

The ω^i_c in equation (19) has two parts: first part is $\omega^i_{c,0}$, the deviation of instability frequency on neutral curve from the frequency in the limit of small n, for the case of perfect open–open boundary conditions (as given by $\omega^i_{c,0}=m\pi/\tau$, where $m=0,\pm1$) and the second part is $\tilde{\omega}^i$, due to the imperfections present in the boundary conditions (that is $\varepsilon_1 r_1$ and $\varepsilon_2 r_2$). Therefore, ω^i_c can be given as $\omega^i_c=\omega^i_{c,0}+\tilde{\omega}^i$. The instability frequency for combustor with non-ideal boundaries, $\omega^i=\omega^i_0+\omega^i_c$ can also be restructured as $\omega^i=\omega^i_{0,t}+\tilde{\omega}^i$, where $\omega^i_{0,t}$ is the instability frequency on the neutral curves for a combustor with perfectly open–open end conditions, $\omega^i_{0,t}=\omega^i_0+\omega^i_{c,0}$. Making use of $\omega^i=\omega^i_{0,t}+\tilde{\omega}^i$, and also assuming smallness of $\tilde{\omega}^i$, in equation (19), we arrive at an explicit expression for $\tilde{\omega}^i$

$$
\tilde{\omega}^i=\frac{\alpha\left[\begin{array}{l}
\varepsilon_1 Re(r_1)\sin\left\{\omega^i_{0,t}(\beta_2-\beta_1)\right\}\\
+\varepsilon_2 Re(r_2)\sin\left\{\omega^i_{0,t}(\beta_1+\beta_2)\right\}
\end{array}\right]}{\left\{\begin{array}{l}
\tau\left[(1+\alpha)\sin\left(\omega^i_{0,t}\beta_1\right)-(1-\alpha)\sin\left(\omega^i_{0,t}\beta_2\right)\right]\\
\times\left\{\sin\left(\omega^i_{0,t}\beta_1\right)-\sin\left(\omega^i_{0,t}\beta_2\right)\right\}
\end{array}\right\}}
\tag{20}
$$

Making use of α, β_1 and β_2, as given by equation (10), equation (20) can be rewritten in a more convenient form which provides dependence on all combustor parameters (flame location, cross-section jump and temperature jump)

$$
\tilde{\omega}^i=\frac{\left(\frac{S_2}{S_1}\frac{\rho_1}{\rho_2}\frac{c_1}{c_2}\right)\left[\begin{array}{l}
-\varepsilon_1 Re(r_1)\sin\left(\dfrac{2\omega^i_{0,t}\left(x_q-L\right)}{c_2}\right)\\
-\varepsilon_2 Re(r_2)\sin\left(\dfrac{2\omega^i_{0,t}x_q}{c_1}\right)
\end{array}\right]}{\left[\begin{array}{l}
\tau\left[\begin{array}{l}
\left(1+\dfrac{S_2}{S_1}\dfrac{\rho_1}{\rho_2}\dfrac{c_1}{c_2}\right)\sin\left\{\omega^i_{0,t}\left(\dfrac{x_q}{c_2}-\dfrac{x_q}{c_1}-\dfrac{L}{c_2}\right)\right\}\\
-\left(1-\dfrac{S_2}{S_1}\dfrac{\rho_1}{\rho_2}\dfrac{c_1}{c_2}\right)\sin\left\{\omega^i_{0,t}\left(\dfrac{L}{c_2}-\dfrac{x_q}{c_1}-\dfrac{x_q}{c_2}\right)\right\}
\end{array}\right]\\
\left[\begin{array}{l}
\sin\left\{\omega^i_{0,t}\left(\dfrac{x_q}{c_2}-\dfrac{x_q}{c_1}-\dfrac{L}{c_2}\right)\right\}\\
-\sin\left\{\omega^i_{0,t}\left(\dfrac{L}{c_2}-\dfrac{x_q}{c_1}-\dfrac{x_q}{c_2}\right)\right\}
\end{array}\right]
\end{array}\right]}
\tag{21}
$$

It is clear from equation (21) that linear perturbation ε_1 and ε_2 at the ends of the combustor perturbs $\omega^i_{c,0}$ linearly (as $\tilde{\omega}^i$ comes out to be small). Inclusion of the cross-section jump into the equation does not change the scenario. However, the effect of temperature jump across flame introduces intricate effects of c_1 and c_2 into trigonometric expressions of equation (21), making it difficult to analyse this equation further. As a matter of simplification, equation (21) can be visualized in a compact form if we assume $S_1=S_2$ and $T_1=T_2$, and thus $c_1=c_2=c$, $\rho_1=\rho_2$

$$
\tilde{\omega}^i=\frac{\left\{\begin{array}{l}
-\varepsilon_1 Re(r_1)\sin\left(\dfrac{2\omega^i_{0,t}\left(x_q-L\right)}{c}\right)\\
-\varepsilon_2 Re(r_2)\sin\left(\dfrac{2\omega^i_{0,t}x_q}{c}\right)
\end{array}\right\}}{2\tau\sin\left(\frac{\omega^i_{0,t}L}{c}\right)\left\{\begin{array}{l}
\sin\left(\dfrac{\omega^i_{0,t}L}{c}\right)\\
-\sin\left(\dfrac{\omega^i_{0,t}\left(2x_q-L\right)}{c}\right)
\end{array}\right\}}
\tag{22}
$$

The corresponding n^i_{th} based on equation (20) can be obtained from equation (18b) as follows

$$n^i_{th} = \frac{\left\{\begin{array}{l} 2\left[(1+\alpha)\sin\left(\omega^i\beta_1\right) - (1-\alpha)\sin\left(\omega^i\beta_2\right)\right] \\ \quad + \varepsilon_1 G_1 + \varepsilon_2 G_2 \end{array}\right\}}{2\cos\left(\omega^i_c\tau\right)\left\{\sin\left(\omega^i\beta_1\right) - \sin\left(\omega^i\beta_2\right)\right\}} \quad (23)$$

where

$$\begin{aligned} G_1 = {} & (1+\alpha)Im(r_1)\cos\left(\omega^i\beta_1\right) \\ & -(1-\alpha)Im(r_1)\cos\left(\omega^i\beta_2\right) \\ & -n^i_{th,0}\left\{\begin{array}{l} Im(r_1)\left(\cos\left(\omega^i\beta_1\right) - \cos\left(\omega^i\beta_2\right)\right)\cos\left(\omega^i_c\tau\right) \\ +Im(r_1)\left(\sin\left(\omega^i\beta_1\right) - \sin\left(\omega^i\beta_2\right)\right)\sin\left(\omega^i_c\tau\right) \\ +Re(r_1)\left(\cos\left(\omega^i\beta_1\right) - \cos\left(\omega^i\beta_2\right)\right)\sin\left(\omega^i_c\tau\right) \end{array}\right\}, \end{aligned}$$

and

$$\begin{aligned} G_2 = {} & (1+\alpha)Im(r_2)\cos\left(\omega^i\beta_1\right) \\ & +(1-\alpha)Im(r_2)\cos\left(\omega^i\beta_2\right) \\ & -n^i_{th,0}\left\{\begin{array}{l} Im(r_2)\left(\cos\left(\omega^i\beta_1\right) + \cos\left(\omega^i\beta_2\right)\right)\cos\left(\omega^i_c\tau\right) \\ +Im(r_2)\left(\sin\left(\omega^i\beta_1\right) - \sin\left(\omega^i\beta_2\right)\right)\sin\left(\omega^i_c\tau\right) \\ +Re(r_2)\left(\cos\left(\omega^i\beta_1\right) + \cos\left(\omega^i\beta_2\right)\right)\sin\left(\omega^i_c\tau\right) \end{array}\right\} \end{aligned}$$

$n^i_{th,0}$ is the threshold of n for ideal open–open end conditions. Equations (20) to (22) suggest that the deviation of instability frequency ($\tilde{\omega}^i$) due to imperfections in the boundary conditions depends linearly on the perturbation parameters ε_1 and ε_2. Thus, the 1D analytical solutions for combustors with open–open end conditions are quite robust, in general. However, from equation (22) we can see that there exists few situations where the analytical solutions might lose their robustness:

(a) When $\sin(\omega^i_{0,t}L/c) = \sin(\omega^i_{0,t}(2x_q - L)/c)$, the flame lies close to $x_q = L$. As per equation (23), the corresponding n^i_{th} goes to infinity. We can say that when n^i_{th} goes to infinity, the aspect of robustness will be irrelevant, as the system is expected to behave as linearly stable for large n. Thus, this case can be treated as not important for practical combustors. The analytical solutions retain their robustness when flame situates close to $x_q = 0$. It can be easily shown that when the flame lies close to either ends for a closed–open combustor, the analytical solution given by Mukherjee and Shrira[21] will lose its robustness.

(b) When $\tau \to 0$, this is the region with numerous small neutral loops of reducing scale, on the left-hand side of the neutral curve. However, we must mention that for this case, as long as $\omega^i_c\tau$ retains its smallness, in spite of large ω^i_c, the solution will retain robustness. Thus, for that case the robustness of n^i_{th} will not be affected, as can be seen from equation (23).

(c) When $\sin(\omega^i_{0,t}L/c) = 0$. This case represents the acoustic mode solution for an open–open combustor with uniform temperature.

The corresponding situations can also be seen from equation (21) for general combustor parameters. These cases when the solutions might lose their robustness need to be studied separately in greater details.

5.1.1. Sensitivity of the neutral curves to complex perturbation of combustor end boundaries. A detailed explanation of the effect of the perturbation on the acoustic end conditions of the open–open combustor on the neutral curves of the intrinsic modes can be provided with the help of Figures 12 and 13. In these figures, the solid line

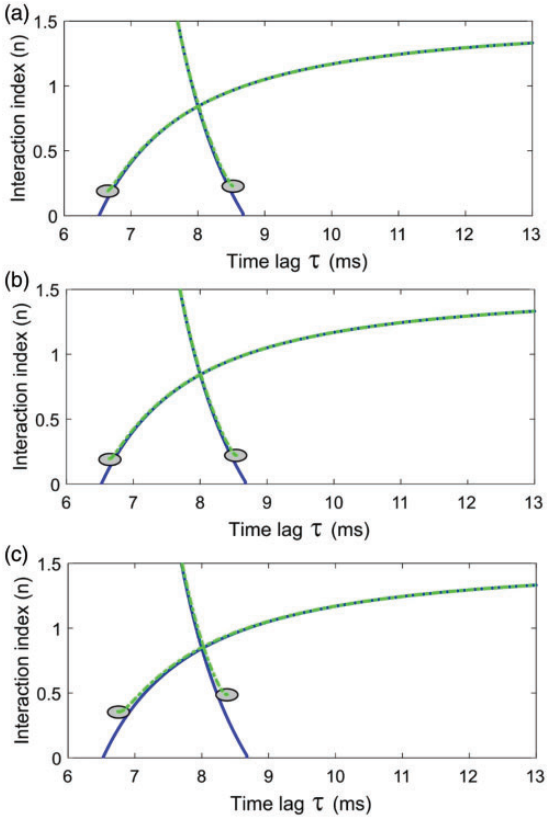

Figure 12. Neutral curves (23) on the $n - \tau$ plane for the second intrinsic mode ($m^i = 1$) of an open–open combustor with uniform temperature and cross-section. Solid lines (blue online) represent the neutral curves for $\varepsilon_1 = 0.0$ and $\varepsilon_2 = 0.0$. Dashed-dotted lines (green online) represent the neutral curves for (a) $\varepsilon_1 = 0.1$, $r_1 = 1.0$, $\varepsilon_2 = 0.0$; (b) $\varepsilon_1 = 0.0$, $\varepsilon_2 = 0.1$, $r_2 = 1.0$ and (c) $\varepsilon_1 = 0.1$, $r_1 = 1.0$, $\varepsilon_2 = 0.1$, $r_2 = 1.0$, respectively. Elliptical dots represent the areas on the neutral curves, where analytical solutions (23) cease to be robust. The parameters are the same as in Figure 2.

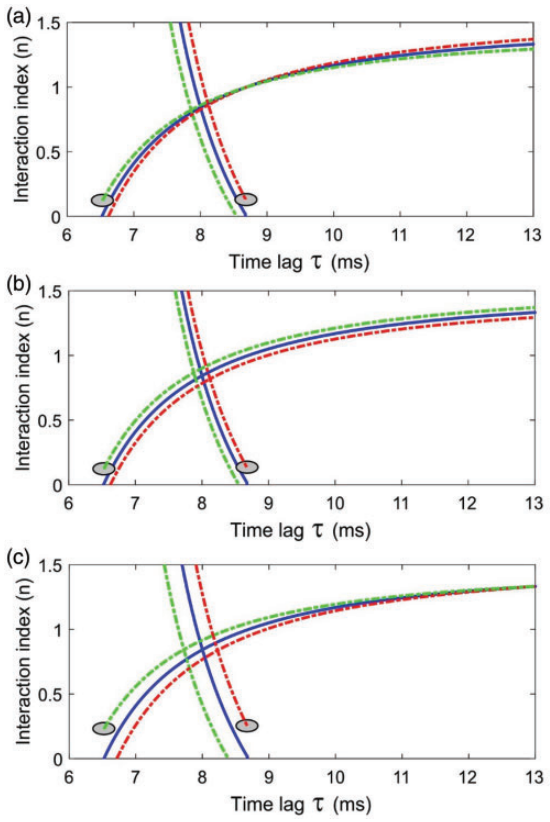

Figure 13. Neutral curves (23) on the $n-\tau$ plane for the second intrinsic mode ($m^i=1$) of an open–open combustor. Light dashed-dotted lines (green online) represent the neutral curves for (a) $\varepsilon_1=0.1$, $r_1=i^*1.0$, $\varepsilon_2=0.0$; (b) $\varepsilon_1=0.0$, $\varepsilon_2=0.1$, $r_2=i^*1.0$ and (c) $\varepsilon_1=0.1$, $r_1=i^*1.0$, $\varepsilon_2=0.1$, $r_2=i^*1.0$ respectively. Dark dashed-dotted lines (red online) represent the neutral curves for (a) $\varepsilon_1=0.1$, $r_1=-i^*1.0$, $\varepsilon_2=0.0$; (b) $\varepsilon_1=0.0$, $\varepsilon_2=0.1$, $r_2=-i^*1.0$ and (c) $\varepsilon_1=0.1$, $r_1=-i^*1.0$, $\varepsilon_2=0.1$, $r_2=-i^*1.0$, respectively. Notations and other parameters are the same as in Figure 12.

(blue online) represents the neutral curve for the second intrinsic mode with ideal open–open end conditions. The elliptical dots indicate the area of the neutral curve when the robustness of the analytical solution (23) does not hold anymore. Panels (a), (b) and (c) in each figure present three different cases when the linear perturbation is assumed for the acoustic end condition of the open end on the left (upstream) to the flame, open end on the right (downstream) to the flame and both the ends, respectively. Thus, for panel (a) $\varepsilon_2=0$, for panel (b) $\varepsilon_1=0$ and for panel (c) both ε_1, ε_2 are non-zero.

In Figure 12, a real perturbation (ε_1 and/or ε_2) of 0.1 is assumed. The light dashed-dotted line (green online) depicts the perturbed solution. In this case, the neutral curve segment corresponding to $\omega_c^i\tau=0$ is very robust. The non-ideal segments almost exactly overlap with the neutral segments $\omega_c^i\tau=0$ for an open–open combustor with ideal end conditions. Analysis of higher values of perturbations (ε_1 and ε_2) has further proved (shown in Section 5.1.3) that the neutral segments $\omega_c^i\tau=\pm\pi$ are less robust. In all these figures, panel (c) demonstrates more sensitivity to end boundary perturbations, as compared to panels (a) and (b). In Figure 13, an imaginary perturbation (ε_1 and/or ε_2) of $\pm i^*0.1$ is assumed. The light dashed-dotted lines (green online) correspond to the neutral curves due to $+i^*0.1$ perturbation, whereas the dark dashed-dotted lines (red online) correspond to the neutral curves due to $-i^*0.1$ perturbation. Due to $+i^*0.1$ perturbation the neutral curve segments shift to the left, whereas to $-i^*0.1$ perturbation the same segments shift to the right, relative to the neutral curve for ideal end conditions. Note that in this case the imaginary perturbation has a more significant impact on all neutral segments than the real perturbation of end conditions.

In general, the assumption of complex perturbation on the acoustic ends of an open–open combustor shows that the neutral segment $\omega_c^i\tau=0$ is very robust, whereas the neutral segments $\omega_c^i\tau=\pm\pi$ are sensitive to small perturbations (will be shown in the next two sections).

5.1.2. Numerical validation of the neutral curves for non-ideal end boundaries. We present numerical validation of the analytical solutions of Section 5.1.1 considering complex perturbation of the end boundaries. Figure 14 shows two cases: (a) without and (b) with temperature and cross-section jump ($T_2/T_1=2.25$, $S_2/S_1=1.5$) with $\varepsilon_1=0.1$, $r_1=1.0+i^*1.0$, $\varepsilon_2=0.1$, $r_2=1.0+i^*1.0$ for the second intrinsic mode. We validate numerically (based on equation (5)) the main neutral loop and the small loop to its nearest left for both cases. The numerical solutions do not take into consideration the switch of mode identities.

Clearly, equation (23) captures the neutral segment $\omega_c^i\tau=0$ quite accurately; however, it fails to capture the neutral curve segment $\omega_c^i\tau=\pi$ with a comparable accuracy. This is found to be a general limitation of the present perturbation method, which does not predict the neutral segments $\omega_c^i\tau=\pm\pi$ with high level of accuracy. For the neutral loops on the left, it fails to capture the neutral segments $\omega_c^i\tau=\pm\pi$ at all. The main reason for this deviation can be seen from equations (20) to (22). The basic assumption of the perturbation method is that small perturbations ε_1, ε_2 in the end boundaries result in small deviation, $\tilde{\omega}^i$, of the instability frequency. This assumption is too restrictive for the neutral curve segments $\omega_c^i\tau=\pm\pi$. Our numerical simulations performed so far (not shown here) show that on the neutral segments $\omega_c^i\tau=\pm\pi$, $\tilde{\omega}^i$ is indeed large, invalidating the basic assumption of the perturbation method implemented here. This calls for an improved

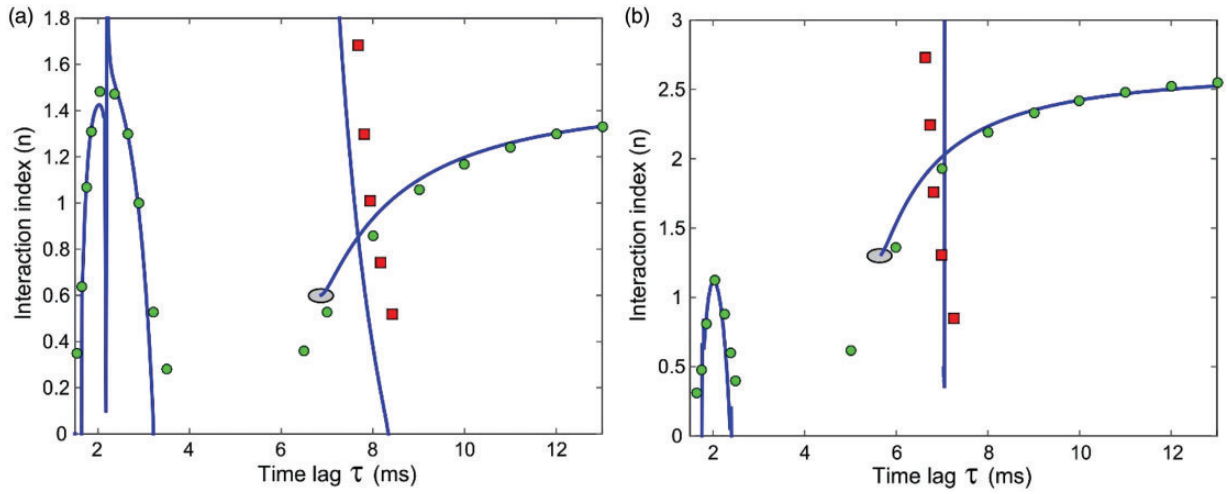

Figure 14. Neutral curves (23) on the $n-\tau$ plane for the second intrinsic mode ($m^i=1$) of an open–open combustor with $\varepsilon_1=0.1$, $r_1=1.0+i^*1.0$, $\varepsilon_2=0.1$, $r_2=1.0+i^*1.0$: (a) without and (b) with temperature and cross-section jump ($T_2/T_1=2.25$, $S_2/S_1=1.5$). Circles (green online) and squares (red online) indicate the numerical solution of intrinsic and acoustic modes, respectively, based on (5). Elliptical dots represent the areas on the neutral curves, where analytical solutions (23) cease to be robust. Notations and other parameters are the same as in Figure 12.

method enabling us to capture the neutral curve segments $\omega_c^i\tau=\pm\pi$ with higher accuracy. This task, however, goes beyond the scope of the present work.

Nonetheless, we can claim that perturbation method does capture $\omega_c^i\tau=0$ segments properly (even for complex perturbation of boundaries). The analytical solutions (equations (20) to (23)) loose robustness when on the $n-\tau$ plane we find two solutions for single time lag (one for $\omega_c^i\tau=\pm\pi$ and another for $\omega_c^i\tau=0$).

5.1.3. Effect on the neutral curve due to transition from open end to anechoic end. Here, we attempt to find out what happens with the neutral curves, when we gradually vary the acoustic end boundaries of a combustor from perfectly reflecting to non-reflecting (or anechoic).

Figure 15 shows the neutral curve for the second intrinsic mode taking into account temperature and cross-section jump ($T_2/T_1=2.25$, $S_2/S_1=1.5$) and $r_1=1.0$, $r_2=1.0$ for six different levels of perturbations of the acoustic end boundaries: (a) $\varepsilon_1=0.1$, $\varepsilon_2=0.1$; (b) $\varepsilon_1=0.2$, $\varepsilon_2=0.2$; (c) $\varepsilon_1=0.3$, $\varepsilon_2=0.3$; (d) $\varepsilon_1=0.5$, $\varepsilon_2=0.5$; (e) $\varepsilon_1=0.7$, $\varepsilon_2=0.7$ and (f) $\varepsilon_1=0.9$, $\varepsilon_2=0.9$. Here, we refrain from considering complex perturbations and stick to real perturbations only. As evident from panels (a) to (d), the neutral curves for $\omega_c^i\tau=0$ are captured with a high level of accuracy almost everywhere. However, the prediction accuracy is not so good for the $\omega_c^i\tau=\pm\pi$ segments, for reasons explained in the previous section. As we perturb the boundaries further by 70% and 90% as seen from panels (e) and (f), the analytical prediction deviates significantly from its numerical counterpart. However, in this range of perturbation, the present method is not expected to work at all. For 100% perturbation (perfectly anechoic end), the neutral curve becomes a straight line (i.e. constant n_{th}^i) parallel to τ axis (as shown in Figures 6 and 7). Nevertheless, the analytical solution captures $\omega_c^i\tau=0$ with remarkable accuracy for reflection coefficients $R_1(0)$ and $R_2(L)$ varying from -1 to -0.5. We anticipate that an equally good prediction can be obtained for $R_1(0)$ and $R_2(L)$ varying from -0.5 to 0, when we implement the same perturbation method for the neutral curves predicted by Hoeijmakers et al.[10] for non-reflecting boundaries. In that process, we can capture the neutral segment $\omega_c^i\tau=0$ with good accuracy for $R_1(0)$ and $R_2(L)$ varying from -1 to 0 (and in the same way from $+1$ to 0, when we migrate from closed end to anechoic end). A better method has to be developed to capture the neutral curves in the domain of two solutions for single time lag on the $n-\tau$ plane. We also observe from Figure 15 that above a certain threshold of perturbation, the neutral segment $\omega_c^i\tau=\pm\pi$ disappears from the window of consideration. What happens is yet to be investigated.

We can certainly claim from our current observations that even for a significant 50% perturbation of the real part of the reflection coefficients of either end of the combustor, the neutral curve segment corresponding to $\omega_c^i\tau=0$ is well captured by the analytical solution (23).

5.2. Growth rate

The instability frequencies and the neutral curve segments $\omega_c^i\tau=0$ for intrinsic modes are found to be quite robust, except a few situations mentioned in the

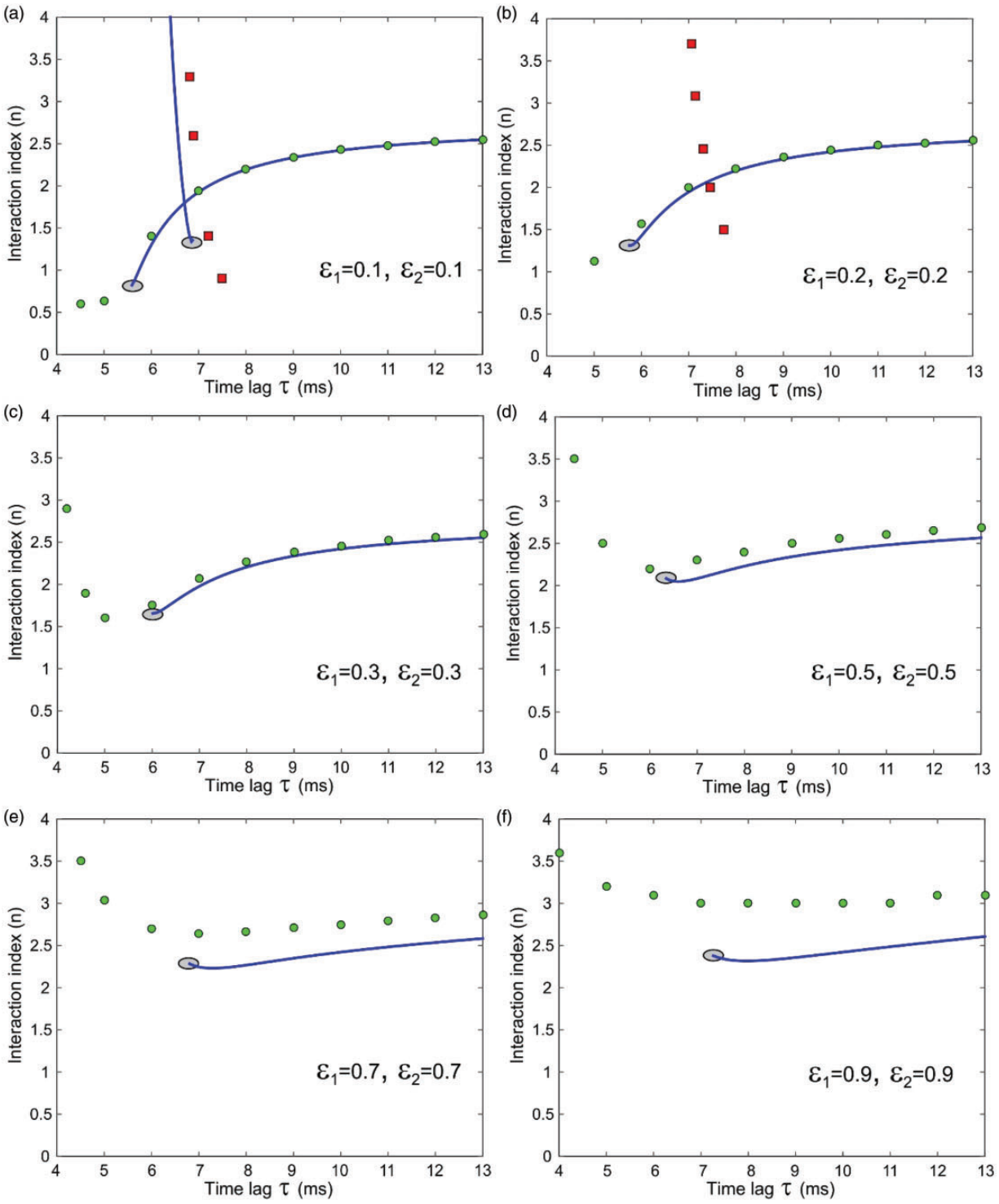

Figure 15. Neutral curves (23) on the $n - \tau$ plane for the second intrinsic mode ($m^i = 1$) of an open–open combustor with temperature and cross-section jump ($T_2/T_1 = 2.25$, $S_2/S_1 = 1.5$) and $r_1 = 1.0$, $r_2 = 1.0$ for: (a) $\varepsilon_1 = 0.1$, $\varepsilon_2 = 0.1$; (b) $\varepsilon_1 = 0.2$, $\varepsilon_2 = 0.2$; (c) $\varepsilon_1 = 0.3$, $\varepsilon_2 = 0.3$; (d) $\varepsilon_1 = 0.5$, $\varepsilon_2 = 0.5$; (e) $\varepsilon_1 = 0.7$, $\varepsilon_2 = 0.7$ and (f) $\varepsilon_1 = 0.9$, $\varepsilon_2 = 0.9$. Circles (green online) and squares (red online) represent the numerical solution of intrinsic and acoustic modes, respectively, based on equation (5). The numerical solutions do not consider the switch of mode identities on the neutral curve. Notations and other parameters are the same as in Figure 12.

previous section. The robustness of the growth rate can be checked, as well. For general boundary conditions $R_1(0)$ and $R_2(L)$, the growth rate expression can be obtained in a similar manner as prescribed in Section 4.3

$$\omega_1^i = \frac{n_1^i e^{i\omega^i\tau}\left[\begin{array}{l}(1-R_1(0)R_2(L))\cos(\omega^i\beta_1)+(R_2(L)-R_1(0))\cos(\omega^i\beta_2)\\ \quad +i\{(1+R_1(0)R_2(L))\sin(\omega^i\beta_1)+(R_2(L)+R_1(0))\sin(\omega^i\beta_2)\}\end{array}\right]}{\left[\begin{array}{l}(1+\alpha)\beta_1\{(1-R_1(0)R_2(L))\sin(\omega^i\beta_1)-i(1+R_1(0)R_2(L))\cos(\omega^i\beta_1)\}\\ +(1-\alpha)\beta_2\{(R_2(L)-R_1(0))\sin(\omega^i\beta_2)-i(R_2(L)+R_1(0))\cos(\omega^i\beta_2)\}\\ -n_{th,0}^i e^{i\omega^i\tau}\left\{\begin{array}{l}(1-R_1(0)R_2(L))(i\tau\cos(\omega^i\beta_1)-\beta_1\sin(\omega^i\beta_1))\\ \quad +(R_2(L)-R_1(0))(i\tau\cos(\omega^i\beta_2)-\beta_2\sin(\omega^i\beta_2))\\ \quad +i(1+R_1(0)R_2(L))(i\tau\sin(\omega^i\beta_1)+\beta_1\cos(\omega^i\beta_1))\\ \quad +i(R_2(L)+R_1(0))(i\tau\sin(\omega^i\beta_2)+\beta_2\cos(\omega^i\beta_2))\end{array}\right\}\end{array}\right]} \tag{24}$$

For obtaining the specific expression for the growth rate of intrinsic modes in an open–open combustor with non-ideal end conditions (17a) and (17b), we plug the expressions of $R_1(0)$ and $R_2(L)$ as per equations (17a) and (17b) in equation (24) and arrive at the following expression

$$\omega_1^i = \frac{2n_1^i e^{i\omega^i\tau}(\sin(\omega^i\beta_1)-\sin(\omega^i\beta_2))+\varepsilon_1 H_1+\varepsilon_2 H_2}{2\left[\begin{array}{l}-(1+\alpha)\beta_1\cos(\omega^i\beta_1)+(1-\alpha)\beta_2\cos(\omega^i\beta_2)\\ -n_{th,0}^i e^{i\omega^i\tau}\left\{\begin{array}{l}i\tau(\sin(\omega^i\beta_1)-\sin(\omega^i\beta_2))\\ +(\beta_1\cos(\omega^i\beta_1)-\beta_2\cos(\omega^i\beta_2))\end{array}\right\}\end{array}\right]} \tag{25}$$

where

$$H_1 = i(Re(r_1)+iIm(r_1)) \times\left[\begin{array}{l}-n_1^i e^{i\omega^i\tau}(\cos(\omega^i\beta_1)-\cos(\omega^i\beta_2))\\ +\omega_{1,0}^i\left\{\begin{array}{l}(1+\alpha)\beta_1\sin(\omega^i\beta_1)-(1-\alpha)\beta_2\sin(\omega^i\beta_2)\\ -n_{th}^i e^{i\omega^i\tau}\left\{\begin{array}{l}i\tau(\cos(\omega^i\beta_1)-\cos(\omega^i\beta_2))-\\ \beta_1\sin(\omega^i\beta_1)+\beta_2\sin(\omega^i\beta_2)\end{array}\right\}\end{array}\right\}\end{array}\right],$$

and

$$H_2 = i(Re(r_2)+iIm(r_2)) \times\left[\begin{array}{l}-n_1^i e^{i\omega^i\tau}(\cos(\omega^i\beta_1)+\cos(\omega^i\beta_2))\\ +\omega_{1,0}^i\left\{\begin{array}{l}(1+\alpha)\beta_1\sin(\omega^i\beta_1)+(1-\alpha)\beta_2\sin(\omega^i\beta_2)\\ -n_{th}^i e^{i\omega^i\tau}\left\{\begin{array}{l}i\tau(\cos(\omega^i\beta_1)+\cos(\omega^i\beta_2))-\\ \beta_1\sin(\omega^i\beta_1)-\beta_2\sin(\omega^i\beta_2)\end{array}\right\}\end{array}\right\}\end{array}\right]$$

$\omega_{1,0}^i$ represents the growth rate of a combustor with ideal open–open end conditions. Clearly, equation (25) tells us that any small perturbation ε_1 and ε_2 will only perturb the growth rate expressions linearly. However, the only restriction to this statement appears due to the lack of robustness of n_{th}^i under certain conditions, as can be seen from expression (25). The robustness of growth rate expression (25) can further be proved using Figure 16 for $m^i = 1$ at $\tau = 9$ ms. The solid line (blue online) shows the growth rate for a combustor with the ideal end conditions and the light dashed-dotted line (green online) represents the growth rate for complex perturbations of acoustic boundaries

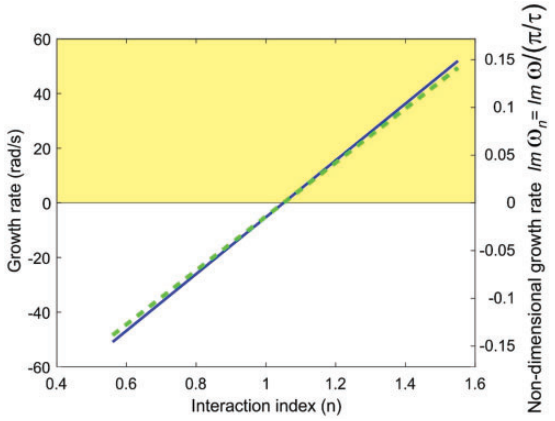

Figure 16. Growth rate for $m^i = 1$ at $\tau = 9$ ms for an open–open combustor with uniform temperature and cross-section. The solid line (blue online) represents the growth rate for $\varepsilon_1 = 0.0$ and $\varepsilon_2 = 0.0$. Light dashed-dotted line (green online) represents the growth rate for $\varepsilon_1 = 0.4$, $r_1 = 1.0 + i*1.0$, $\varepsilon_2 = 0.4$, $r_2 = 1.0 + i*1.0$. The overlapping nature of these two solutions proves the robustness of equation (25) for this case. The instability domain is lightly shaded (yellow online). The parameters of the system are the same as in Figure 12.

given by $\varepsilon_1 = 0.4$, $r_1 = 1.0 + i*1.0$, $\varepsilon_2 = 0.4$, $r_2 = 1.0 + i*1.0$. The two lines almost overlap with each other (even for 40% perturbation of the boundary conditions), verifying that in this case, solution (25) of the growth rate is indeed robust. However, this is not true for all the cases. Figure 12 shows that for $\tau = 9$ ms, we have solution for the intrinsic mode corresponding to $\omega_c^i \tau = 0$ and this neutral segment is also found to be very robust, as explained in Section 5.1.2. Thus, in this case, the robustness of the neutral curve ensures the robustness of the growth rate. However, when the neutral curves are not robust, particularly near and within the domain of two solutions for single time lag, equation (25) will lose robustness.

In this section, we have checked the robustness of our analytical solutions for intrinsic flame instability for an open–open combustor. We found that the solutions are generally quite robust for all but two cases, when considering all the flame and combustor parameters: the first case is when the flame is located near $x_q = L$ and the second case is when, on the neutral curve, we attain a condition of $\sin(\omega_{0,t}^i L/c) = 0$. Furthermore, the neutral curve segment $\omega_c^i \tau = 0$ is very robust, whereas the robustness study of the segments $\omega_c^i \tau = \pm\pi$ requires more attention in future.

6. Effect of parameters (flame location, cross-section jump, temperature jump) on stability behaviour of intrinsic modes in open–open combustors

As per equations (13) and (16), the threshold in n and growth rate depend on various combustor parameters. In this section, we try to find how n_{th}^i and growth rate depend on the three main parameters of an open–open combustor model: (i) cross-section jump, (ii) temperature jump and (iii) flame location. It is also a matter of prime interest to find out whether for certain parameter domain the n-threshold decreases or growth rate increases.

Figure 17 plotted on the basis of equation (13) illustrates the effect of cross-section jump on the neutral curve main loop. The temperature jump across the flame is neglected and the flame is assumed to lie at $x_q = L/3$. The figure shows two different cases of cross-section jump: (1) $S_2/S_1 = 1$ and (2) $S_2/S_1 = 2$. Region (i) (lavender online) indicates the instability domain for $S_2/S_1 = 1$. The common domain of instability (ii) is lightly shaded (yellow online). In all subsequent figures, the common instability domain is also lightly shaded (yellow online). It can be seen from the figure that inclusion of cross-section jump lifts the overall neutral curve and shifts it slightly to the right. This means that the n-threshold of intrinsic

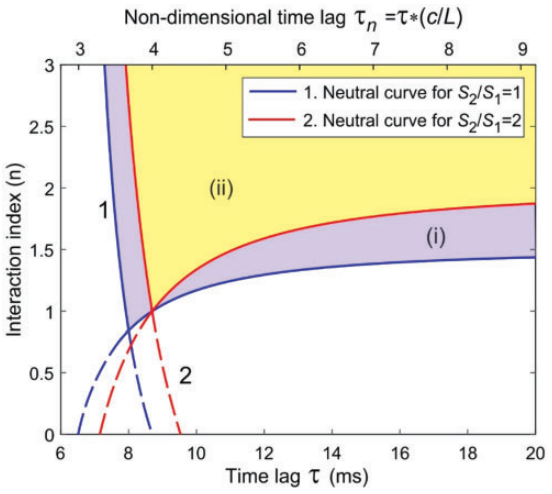

Figure 17. Effect of cross-section jump on the stability domain for $m^i = 1$, $x_q = L/3$ and uniform temperature. The plot is based on equation (13) and shows stability domain (1) with no jump ($S_2/S_1 = 1$) and stability domain (2) with ($S_2/S_1 = 2$) cross-section jump. Region (i) (lavender online) marks the instability domains for the case $S_2/S_1 = 1$. The common instability domain (ii) for these two cases is lightly shaded (yellow online). Other parameters are the same as in Figure 6(a).

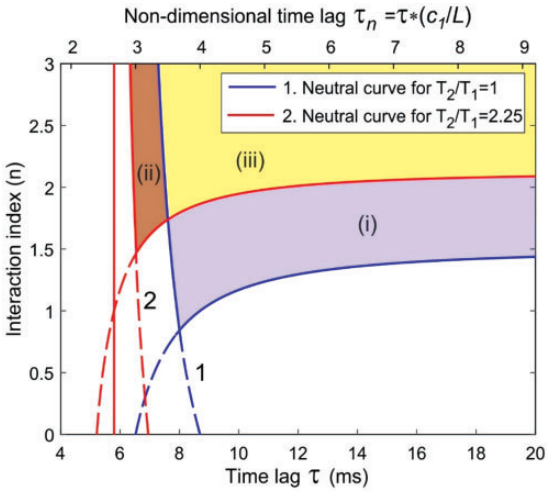

Figure 18. Effect of temperature jump on stability domain for $m^i = 1$, $x_q = L/3$ and uniform cross-section. The plot is based on equation (13) and shows configurations: (1) with no jump, i.e. $T_2/T_1 = 1$ (or $c_2/c_1 = 1$)) and (2) with $T_2/T_1 = 2.25$ (or $c_2/c_1 = 1.5$)) temperature jump. Regions (i) (lavender online) and (ii) (brown online) indicate the instability domains for the cases $c_2/c_1 = 1$ and $c_2/c_1 = 1.5$, respectively, with the common instability domain being lightly shaded (yellow online) (iii). Other parameters are the same as in Figure 6(a).

instability gets lifted due to cross-section jump, at least in this case.

The effect of temperature jump on $n_{th}^i(\tau)$ is somewhat different. Figure 18, plotted on the basis of equation

(13), compares two different cases of temperature jump: (1) for $T_2/T_1 = 1$ (or $c_2/c_1 = 1$) and (2) $T_2/T_1 = 2.25$ (or $c_2/c_1 = 1.5$). The cross-section jump is neglected and the flame is assumed to lie at $x_q = L/3$. The temperature jump lifts the neutral curve in general and also stretches the span of the neutral loop to the left. Hence, the inclusion of temperature jump in the system increases the n^i_{th} for all time lags in this case. Note that in Figure 18 there is a vertical neutral curve segment corresponding to $\omega^i_c \tau = \pi$ for the case $T_2/T_1 = 2.25$ on the left side. Hence, in contrast to Figure 6(a), in this figure we see two neutral segments corresponding to $\omega^i_c \tau = \pi$ for the case $T_2/T_1 = 2.25$. This phenomenon is due to intrinsic–acoustic mode coupling. On the immediate right-hand side of this vertical $\omega^i_c \tau = \pi$ segment, we have two solutions (i.e. two neutral segments) for a specific τ. On the immediate left side, we have only one solution for a specific τ. Further details of this aspect will be reported elsewhere.

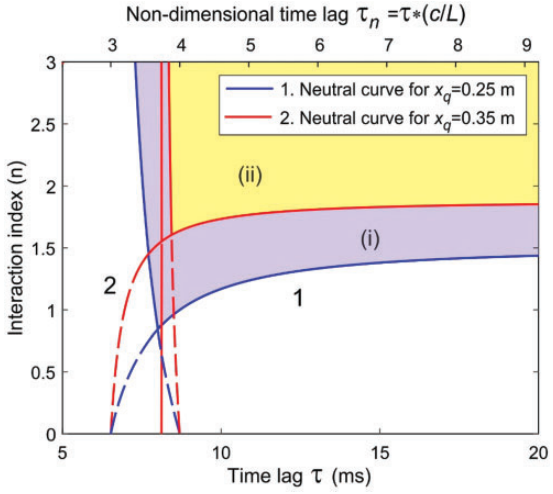

Figure 19. Effect of flame location on stability domain for $m^i = 1$. The temperature and cross-section are uniform. The plot is based on equation (13) and shows two flame locations: (1) $x_q = 0.25$ m and (2) $x_q = 0.35$ m. The instability domains for $x_q = 0.25$ m is marked by (i) (lavender online). The common instability domain for these two cases, (ii), is lightly shaded (yellow online). Other parameters are the same as in Figure 6(a).

Figure 19, plotted on the basis of equation (13), demonstrates the effect of flame location on $n^i_{th}(\tau)$. The figure is drawn for two different flame locations: (1) $x_q = 0.25$ m and (2) $x_q = 0.35$ m, under the assumption of no temperature and cross-section jumps. Region (i) (lavender online) represents the instability domain for $x_q = 0.25$ m. The neutral curve shifts slightly up as the flame is shifted from $x_q = 0.25$ m to $x_q = 0.35$ m. In other words, the n-threshold increases as the flame is moved from $x_q = 0.25$ m to $x_q = 0.35$ m. Further analytical studies (not reported here) confirm that this is indeed a general trend: an increase of x_q always increases n-threshold.

A similar parametric study can be performed for the growth rates of the intrinsic modes, as well. Figure 20(a) and (b) shows the effect of cross-section jump and temperature jump, respectively, on the growth rate. The flame is assumed to be located at $x_q = L/3$. Growth rates are calculated using the explicit analytical

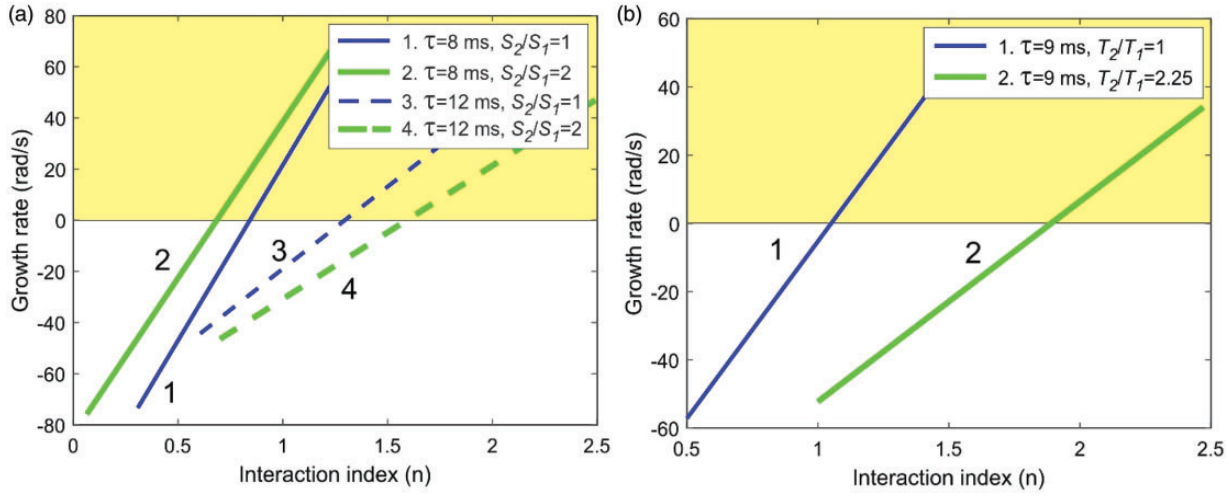

Figure 20. Effect of cross-section jump and temperature jump on growth rates for $m^i = 1$, $x_q = L/3$ (based on equation (16)). (a) Two different time lags (8 and 12 ms) are indicated by solid and dashed lines. Two values of cross-section jumps ($S_2/S_1 = 1$ and $S_2/S_1 = 2$) are marked in dark (blue online) and light (green online). The temperature is assumed to be uniform for this case. (b) Two values of temperature jump $T_2/T_1 = 1$ (or $c_2/c_1 = 1$) and $T_2/T_1 = 2.25$ (or $c_2/c_1 = 1.5$) are marked in dark (1) (blue online) and light (2) (green online) for time lag = 9 ms. The cross-section is assumed uniform for this case. Other parameters and notation are the same as in Figure 6(a). Lightly shaded region (yellow online) marks the domain of instability.

solution (16). Figure 20(a) shows two different cases for the time lag (8 ms and 12 ms), where cross-section jumps of $S_2/S_1 = 1$ and $S_2/S_1 = 2$ are considered for each case (assuming uniform temperature). The growth rate decreases due to cross-section jump both for the time lag of 8 ms and 12 ms. Dependence of the growth rates on the temperature jumps is illustrated by Figure 20(b): for a single time lag ($\tau = 9$ ms) and uniform cross-section. The figure compares the effect of a moderate temperature jump ($T_2/T_1 = 2.25$ or $c_2/c_1 = 1.5$) with the configuration of no temperature jump ($T_2/T_1 = 1$). The introduction of temperature jump reduces the growth rate (at least for the chosen τ). A similar analysis can be carried out to describe the effect of flame location, as well.

Thus, by manipulating the system parameters like cross-section jump, temperature jump and flame location, we can increase/decrease the n_{th}^i and decrease/increase the growth rate, and hence dampen/instigate the intrinsic mode instability. The flame location for small x_q is found to be most critical for intrinsic flame instability.

7. Conclusions

In the current work, we have analytically studied the features of flame intrinsic modes within a 1D open–open combustor with a linear $n-\tau$ model of heat release. Previous studies by Hoeijmakers et al.[10] and by Mukherjee and Shrira[21] have shown that there is always an infinite number of intrinsic modes present in combustors. Mukherjee and Shrira[21] have shown that for small n these modes are strongly damped for any combustor (i.e. they are very much localized and do not feel combustor boundaries). However, their work on closed–open combustors shows that these modes have the potential to become unstable beyond a certain threshold in n. In this paper, we extend the analysis of Mukherjee and Shrira[21] to open–open combustors with ideal and non-ideal end boundaries and make these salient observations:

(i) We have shown that the phenomenon of 'decoupling', or factorization of the dispersion relation on the neutral curve, found by Mukherjee and Shrira[21] for the ideal closed–open combustors, also occurs for only two other combinations of boundary conditions, (a) ideal open–open and (b) ideal closed–closed. Due to the decoupling of the dispersion relation on the neutral curve, the intrinsic mode incipient instability frequency, for these cases, is found to be independent of the flame location and the combustor parameters. Based on this observation, we have performed a comprehensive study of intrinsic instability of an important common model of combustor, the ideal open–open. However, it is noteworthy that once the non-ideal boundaries of the combustors are considered, this decoupling phenomenon ceases to exist.

(ii) Similar to the findings of Mukherjee and Shrira[21] for closed–open combustors, we have shown here for open–open combustors that for certain bands of τ each intrinsic mode becomes unstable above a certain threshold of n. The threshold depends on the combustor parameters and is explicitly given by equation (13). The neutral curve for each intrinsic mode is qualitatively similar to that of the closed–open model. It consists of combinations of neutral curve segments $\omega_c^i\tau = 0$, $\omega_c^i\tau = \pi$ and $\omega_c^i\tau = -\pi$, where ω_c^i is the discrepancy between the real part of the frequency on the neutral curve and the real part of the frequency in the limit of small n. The neutral curve has two principal segments: one large loop on the extreme right (for larger time lag) and a series of smaller loops of reducing τ scale for the smaller time lag. The large neutral loop on the extreme right consists of neutral segments $\omega_c^i\tau = 0$ and $\omega_c^i\tau = \pi$ only. The neutral curve segment $\omega_c^i\tau = -\pi$ does not feature there. This aspect is qualitatively different to closed–open combustors as reported by Mukherjee and Shrira,[21] where the large neutral loop on the extreme right consists of all the neutral segments $\omega_c^i\tau = 0$, $\omega_c^i\tau = \pi$ and $\omega_c^i\tau = -\pi$, while the main neutral curve loops for each mode are confined to a certain interval in τ for closed–open combustors, the loops and, hence, the instability domains for the open–open systems are not bounded on the large τ side. Thus, beyond a certain time lag, the intrinsic mode is always unstable for open–open combustors. The first intrinsic mode is found to provide the upper bound of the stability domain. Any point on the $n-\tau$ plane that is above this upper bound is guaranteed to be unstable for at least one or multiple intrinsic modes. Most importantly, the intrinsic modes (and also the acoustic modes that get coupled to them) can become unstable at a much lower n-threshold than for a flame in an infinite tube.[10] Moreover, some evidence has been reported in this work to claim that in certain $n-\tau$ parameter space, intrinsic instability might be stronger than the acoustic instability. We have also derived an explicit analytical formula to predict the growth rates for each intrinsic mode. The neutral curves and the growth rate predictions have been validated by numerics.

(iii) The intrinsic flame instabilities as a function of combustor parameters like the flame location, the cross-section and temperature jump across

the flame have been described analytically. By manipulating the system parameters like cross-section jump, temperature jump and flame location, and employing these formulae, combustor designers can increase the n_{th}^i and decrease the growth rate and hence prevent/control the intrinsic mode instability.

(iv) We have analysed the effect of imperfect end conditions on the analytical results of instability frequency, n-threshold and the growth rate of flame intrinsic modes for an open–open combustor. The analytical results described for ideal open–open end boundaries have been found to be generally quite robust, except for the following two cases (for uniform temperature and cross-section):
   (a) The flame lies near the downstream end ($x_q = L$) for an open–open combustor. When the flame resides near the upstream end ($x_q = 0$), the analytical solutions retain their robustness.
   (b) When on the neutral curve $\sin(\omega_{0,t}^i L/c) = 0$ for an open–open combustor (and $\cos(\omega_{0,t}^i L/c) = 0$ for a closed–open combustor), where $\omega_{0,t}^i$ is the instability frequency on the neutral curves for a combustor with perfect end conditions.

The domain on the $n - \tau$ plane with two solutions for a single time lag is found to be not so robust: slight perturbations of the end conditions significantly perturb the neutral segments $\omega_c^i \tau = \pm\pi$ (and also those corresponding to $\omega_c^i \tau = 0$). The reason for this is that the robustness analysis performed here is based on a perturbation method, which in turn is based on the assumption of small deviation, $\tilde{\omega}^i$, of the instability frequency, for small perturbation of combustor boundaries ε_1, ε_2. This assumption is not always valid in the domain of two solutions for single time lag on the $n - \tau$ plane. Remarkably, the neutral segment corresponding to $\omega_c^i \tau = 0$ and the corresponding growth rate are found to be very robust between the points of intersections of the neutral curve segments. We managed to capture the neutral segment $\omega_c^i \tau = 0$ quite accurately even for a significant 50% perturbation of the real part of the reflection coefficients of either end of the combustor. It will require a dedicated effort to derive analytical corrections to the 'ideal' solutions for the cases when the solutions are not robust. The effect of temperature jump on the robustness of the analytical solution is found to be an intricate matter to analyse. This aspect also needs to be dealt with in future studies.

The above conclusions were obtained within the framework of the $n - \tau$ model. Its degree of validity in the range of large (or even moderate) n is not a core matter of investigation here and goes beyond the scope of the current paper. Here, we assume large n to be of O(1). We hope that the obtained results capture at least qualitatively the dependence of intrinsic instabilities on the set of combustor parameters. We also stress that here we have found intrinsic instabilities in the range of relatively small n. At least this subset of the results is expected to survive in more accurate models.

The present work is focused on the analytical study of an open–open combustor with ideal and non-ideal boundary conditions. The coexistence of intrinsic and acoustic modes within a combustor and, hence, a possible coupling between these modes opens a new research topic in combustion instability. It is known from the literature[40] that in a Rijke tube (open–open thermo-acoustic system) there is an audible sound which is a manifestation of thermo-acoustic instability, when the heat source is at the lower half of the tube. This observation implies that the dominant acoustic mode instabilities are subdued for the heat sources (e.g. flame) located in the upper half of the tube. (However, please note that the classical Rijke tube is not a premixed flame configuration.) This gives the flame intrinsic modes of the system a chance to drive the combustion instability, an aspect which calls for further investigation. Once we have established basic properties of intrinsic modes in the open–open combustors, a study of the nonlinear dynamics of the intrinsic modes and their nonlinear interactions with the acoustic modes in an open–open combustor is a logical next step. The mean flow could be also introduced into our analysis without the need to radically change the mathematical framework. The interaction between intrinsic modes of really low frequency and hydrodynamic modes should also be a topic of interest.

Acknowledgement

I gratefully acknowledge the discussions with Prof. Victor Shrira and his valuable comments on the drafts of the paper. The work is a part of the Marie Curie Initial Training Network *Thermo-acoustic and aero-acoustic nonlinearities in green combustors with orifice structures* (TANGO).

Declaration of Conflicting Interests

The author(s) declared no potential conflicts of interest with respect to the research, authorship, and/or publication of this article.

Funding

The author(s) disclosed receipt of the following financial support for the research, authorship, and/or publication of this article: I gratefully acknowledge the financial support from the European Commission under call FP7-PEOPLE-ITN-2012.

References

1. Warren GB. Fuel-economy gains from heated lean air-fuel mixtures in motorcar operation (65-WA/APC-2). *Mech Eng* 1966; 88: 84.

2. Lee RC and Wimmer DB. Exhaust emission abatement by fuel variations to produce lean combustion. *SAE Trans* 1968; 77: 175.
3. Putnam AA. *Combustion driven oscillations in industry*. New York: American Elsevier Publishers, 1971.
4. Mcmanus K, Poinsot T and Candel SM. A review of active control of combustion instabilities. *Prog Energy Combust Sci* 1993; 19: 1–29.
5. Poinsot T, Chatelier CL, Candel SM, et al. Experimental determination of the reflection coefficient of a premixed flame in a duct. *J Sound Vib* 1986; 107: 265–278.
6. Lieuwen T and Yang V. *Combustion instabilities in gas turbine engines: operational experience, fundamental mechanisms, and modeling*. Reston, VA: (AIAA progress in astronautics and aeronautics). 2005.
7. Poinsot T and Veynante D. *Theoretical and numerical combustion*, 3rd ed. Philadelphia, USA: R.T. Edwards, 2011.
8. Dowling AP. The calculation of thermo-acoustic oscillations. *J Sound Vib* 1995; 180: 557–581.
9. Dowling AP and Stow SR. Acoustic analysis of gas turbine combustors. *J Propul Power* 2003; 19: 751–764.
10. Hoeijmakers M, Kornilov V, Arteaga IL, et al. Intrinsic instability of flame-acoustic coupling. *Combust Flame* 2014; 161: 2860–2867.
11. Hoeijmakers M. *Flame-acoustic coupling in combustion instabilities*. PhD Thesis, Technical University of Eindhoven, 2014.
12. Emmert T, Bomberg S and Polifke W. Intrinsic thermoacoustic instability of premixed flames. *Combust Flame* 2015; 162: 75–85.
13. Courtine E, Selle L and Poinsot T. DNS of intrinsic thermoacoustic modes in laminar premixed flames. *Combust Flame* 2015; 162: 4331–4341.
14. Emmert T, Bomberg S, Jaensch S, et al. Acoustic and intrinsic thermo-acoustic modes of a premixed combustor. In: *36th International symposium on combustion*, Seoul, Korea, 31 July–5 August 2016.
15. Hoeijmakers M, Kornilov V, Arteaga IL, et al. Flame dominated thermo-acoustic instabilities in a system with high acoustic losses. *Combust Flame* 2016; 169: 209–215.
16. Bomberg S, Emmert T and Polifke W. Thermal vs acoustic response of velocity sensitive premixed flames. *Proc Combust Inst* 2015; 35: 3185–3192.
17. Kaess R, Polifke W, Poinsot T, et al. CFD based mapping of the thermo-acoustic stability of a laminar premix burner. In: *Proceedings of the summer program*, 2008, pp. 289–302.
18. Gentemann A and Polifke W. Scattering and generation of acoustic energy by a premix swirl burner. In: *ASME turbo expo*, Montreal, Canada, GT2007-27238, 14–17 May 2007.
19. Courtine E, Selle L, Nicoud F, et al. Causality and intrinsic thermo-acoustic instability modes. In: *Proceedings of the summer program*, Stanford University, 6 July–1 August 2014, Centre for Turbulent Research, 2014.
20. Silva CF, Emmert T, Jaensch S, et al. Numerical study on intrinsic thermo-acoustic instability of a laminar premixed flame. *Combust Flame* 2015; 162: 3370–3378.
21. Mukherjee NK and Shrira V. Intrinsic flame instabilities in combustors: analytic description of a 1-D resonator model. *Combust Flame* 2017; 185: 188–209.
22. Hoeijmakers M, Kornilov V, Arteaga IL, et al. Flames in context of thermoacoustic stability bounds. *Proc Combust Inst* 2015; 35: 1073–1078.
23. Drazin PG and Reid WH. *Hydrodynamic stability*, 2nd ed. Cambridge: Cambridge University Press, 2004.
24. Crocco L and Cheng SI. *Theory of combustion instability in liquid propellant rocket motors*. Kingsway, London: Butterworths Scientific Publications, 1956.
25. Lamarque N and Poinsot T. Boundary conditions for acoustic eigenmode computations in gas turbine combustion chambers. *AIAA J* 2008; 46: 2282–2292.
26. Munjal ML. *Acoustics of ducts and mufflers*. New York: John Wiley, 1987.
27. Silva C, Duran I, Nicoud F, et al. Boundary conditions for the computation of thermo-acoustic modes in combustion chambers. *AIAA J* 2014; 52: 1180–1193.
28. Marble F and Candel S. Acoustic disturbances from gas nonuniformities convected through a nozzle. *J Sound Vib* 1977; 55: 225–243.
29. Mukherjee NK, Heckl MA and Shrira V. Analysis of flame intrinsic modes in a resonator. In: *23rd International congress on sound and vibration*, Athens, Greece, 10–14 July 2016.
30. Polifke W, Paschereit CO and Dobbeling K. Constructive and destructive interference of acoustic and entropy waves in a premixed combustor with a choked exit. *Int J Acoust Vib* 2001; 6: 135–146.
31. Kinsler LE, Frey AR, Coppens AB, et al. *Fundamentals of acoustics*, 4th ed. New York: John Wiley & Sons, 2000.
32. Bauerheim M, Nicoud F and Poinsot T. Theoretical analysis of the mass balance equation through a flame at zero and non-zero Mach numbers. *Combust Flame* 2015; 162: 60–67.
33. Truffin K and Poinsot T. Comparison and extension of methods for acoustic identification of burners. *Combust Flame* 2005; 142: 388–400.
34. Schuller T, Durox D, Palies P, et al. Acoustic decoupling of longitudinal modes in generic combustion systems. *Combust Flame* 2012; 159: 1921–1931.
35. Vishnu R, Sujith RI and Aghalayam P. Role of flame dynamics on the bifurcation characteristics of a ducted V-flame. *Combust Sci Technol* 2015; 187: 894–905.
36. Mukherjee N, Heckl MA, Bigongiari A, et al. Nonlinear dynamics of a laminar V flame in a combustor. In: *22nd International congress on sound and vibration*, Florence, Italy, 12–15 July 2015.
37. Silva CF, Merk M, Komarek T, et al. The contribution of intrinsic thermoacoustic feedback to combustion noise and resonances of a confined turbulent premixed flame. *Combust Flame* 2017; 182: 269–278.
38. Mukherjee NK. *Analytic study of intrinsic flame and coupled-intrinsic acoustic instabilities in combustor models*. PhD Thesis, Keele University, 2017.
39. Levine H and Schwinger J. On the radiation of sound from an unflanged circular pipe. *Phys Rev* 1948; 73: 383–406.
40. Rijke PL. On the vibration of the air in a tube open at both ends. *Philos Mag* 1859; 17: 419–422.